Titre: Title:	Crystal chemistry and thermodynamic modelling of the $Al_{13}(Fe,TM)_4$ solid solutions (TM = Co, Cr, Ni, Pt)
Auteurs: Authors:	Paul Lafaye, Kentaro Oishi, Maxime Bourdon, & Jean-Philippe Harvey
Date:	2022
Type:	Article de revue / Article
Référence: Citation:	Lafaye, P., Oishi, K., Bourdon, M., & Harvey, J.-P. (2022). Crystal chemistry and thermodynamic modelling of the $Al_{13}(Fe,TM)_4$ solid solutions (TM = Co, Cr, Ni, Pt). Journal of Alloys and Compounds, 165779. https://doi.org/10.1016/j.jallcom.2022.165779

Crystal chemistry and thermodynamic modelling of the $Al_{13}(Fe,TM)_4$ solid solutions (TM = Co, Cr, Ni, Pt)

Paul Lafaye[a,1], Kentaro Oishi[a], Maxime Bourdon[b], J-P Harvey[a]

[a]CRCT- Polytechnique Montréal, Chem. Eng., Box 6079, Station Downtown, Montréal, Qc, H3C 3A7, Canada
[b]Setaram - Lyon, France

Abstract

The crystal chemistry of the $Al_{13}(Fe,TM)_4$ (TM = Co, Cr, Ni, Pt) solid solutions has been investigated by combining formation enthalpy measurements by differential scanning calorimetry (DSC), density functional theory (DFT) calculations and thermodynamic modelling. The formation enthalpies of seven alloys of the $Al_{13}(Fe,Co)_4$ solid solution were measured by DSC at 920 K, allowing the determination of the mixing enthalpy of the solution. These measurements are presented here for the first time and highlight the ideal nature of this solid solution. In addition, the mixing enthalpy of the $Al_{13}(Fe,TM)_4$ solid solutions (TM = Co, Cr, Ni, Pt) was determined by DFT at 0 K. These calculated and measured data (in the case of the $Al_{13}(Fe,Co)_4$ solid solution) were used to perform thermodynamic modelling of the solid solutions and better understand their thermodynamic stability. In addition, our modelling was used to calculate the TM occupancy on the Fe sites of the $Al_{13}(Fe,TM)_4$ solid solution structure at different temperatures. These data were used to quantify the chemical ordering of the solid solutions as a function of temperature. While these solid solutions show significant chemical ordering at low temperatures, only the $Al_{13}(Fe,Pt)_4$ solution remains highly ordered at high temperatures. These data are presented for the first time in this paper and have allowed us to design an optimal sublattice (SL) model for the $Al_{13}Fe_4$ solid solutions.

[1] Corresponding author, email address: paul.lafaye@polymtl.ca

1. Introduction

Iron is one of the most common impurities found in aluminium alloys. It is present in large amount in the bauxite raw material used to produce primary aluminium [1]. It is also a difficult element to remove upon recycling of aluminium scrap because of its relative nobleness [1, 2, 3]. As a direct consequence, the Fe content tends to increase as the aluminium alloy is recycled by conventional methods if primary metal dilution strategies are not used [2]. The Fe content in Al alloys is usually tightly tracked in order to control the precipitation of brittle Al-Fe intermetallic compounds such as the $Al_{13}Fe_4$ intermetallic phase (monoclinic phase with C2/m space group). This intermetallic can have detrimental effects on the mechanical behaviour of aluminium alloys [1, 3, 4]. The plate-like morphology of the $Al_{13}Fe_4$ precipitates [5, 6] forms crack initiation sites which reduce the mechanical strength of the alloy [7, 8]. In other specific applications, the presence of Fe in aluminium alloys is promoted to improve their corrosion resistance [9, 10] and to increase their hardness [10, 11, 12] in temperature ranges higher than for conventional aluminium alloys applications [10, 12]. In this case, it is essential to optimise the microstructure of these iron-containing aluminium alloys to enhance their mechanical properties while preserving a high corrosion resistance and hardness at high temperature. To do so, several alloying elements such as Mn [12, 13, 14], Ni [12, 15, 16], Cr [12] and Co [12] can be added to the material to refine the coarse structure of the $Al_{13}Fe_4$ precipitates and to strengthen the material. The $Al_{13}Fe_4$ intermetallic is also of major interest for catalytic applications as a new environmentally friendly alternative to Pd-based materials to promote hydrogenation reactions. It can be used as a catalyst with [17] or without [18] Pt additions.

In this context, it is of prime importance to be able to predict the thermodynamic stability of this phase as a function of both the temperature and the chemical composition in order to tune the chemistry of the targeted material for a given application. A reliable prediction of the phase assemblage in multicomponent systems can be achieved using the Calphad approach [19]. Within this approach, the energetic behaviour of each stable/metastable phase is defined using an adequate thermodynamic model [19]. For solid solutions, a class of thermodynamic models used for the description of their free energy are called sub-lattice (SL) models. A well-known example of such a SL model is called the Compound Energy Formalism (CEF) [20]. SL models can be designed after a rigorous analysis of the crystal structure of the considered solid solution. In addition, the crystal chemistry of the solution at the origin of its non-stoichiometry (such as the presence of vacancies or substitutional/interstitial defects) must be characterised to complete the definition of the model.

A key parameter to describe the crystal chemistry is the occupancy of each crystal site by different elements (or vacancies) as a function of composition and temperature. In many instances, the merging of crystal sites exhibiting similar occupancies over a wide range of temperature and chemical composition is required to reduce the complexity of the model. Indeed, a high number of atomic sites may result in the definition of an unacceptably large number of solution components (also called end-members). Nevertheless, in many cases, such crystal chemistry data are lacking in the literature, which greatly limits the construction of the SL model of a given solid solution. The elaboration of the SL model is of crucial importance as an inadequate SL definition will inexorably lead to an inaccurate evaluation of the configurational entropy of mixing of the solution. This entropy contribution will have in turn to be compensated by some excess terms which will likely cause interpolation/extrapolation problems. This is specifically the case for the $Al_{13}(Fe,TM)_4$ solid solution for which no quantitative study about site occupancies have yet been presented. Pang *et al.* [12] are the only authors to have reported that Co and Ni preferentially occupy site Fe(1) of this structure, while Cr and Mn ’ ” ‡ ˆ ‡ ” ‡ • – ‹ ƒ Ž Ž › ‘ … … — ’ › • ‹ – ‡ ‡ w — • ‹ • ‰ ” ‹ • t sï • ä• ‘ –‘ƒ™– ‡ ˜‡ ”ã‘ ” – Š ƒ – ‡ ‹ … ‡ calculations were performed at 0 K by substituting a single atom and therefore do not allow to characterise the crystal chemistry of the solid solution in the whole chemical composition range and at all temperature. In another study, Yamada *et al.* [17] showed that Pt preferentially occupies site Fe(1). Therefore, SL models available in the literature such as the model developed by Sundman *et al.* [22] or, more recently, by Fang *et al.* [4] suffer from important limitations as it will be discussed here. One should also note that the recommendation to define SLs by merging crystal sites with equivalent coordination number [19] is not applicable for the $Al_{13}Fe_4$ phase as it does not allow to reproduce the chemical ordering observed at the stoichiometric composition [4]. Based on this SL model, the phase will be regarded as a solid solution at the $Al_{13}Fe_4$ stoichiometry providing a thermodynamic behaviour radically different from that of an ordered compound, due to the configurational entropy of mixing contribution.

The aim of this paper is to design a robust SL model for the description of the $Al_{13}(Fe,TM)_4$ solid solution that can be extended to higher order systems. To do so, TM site occupancies (TM = Co, Cr, Ni, Pt) in the $Al_{13}(Fe,TM)_4$ solid solution are computed at different temperatures by integrating Density Functional Theory (DFT) calculations presented in this paper to the CEF. This formalism uses the Bragg-Williams approximation [23] for the description of the configurational entropy of mixing for each sublattice. Formation enthalpy measurements of the $Al_{13}(Fe,Co)_4$ solid solution were also carried out at 920 K by *in-situ* synthesis from high-purity metals in a differential scanning calorimeter (DSC).

These new data allowed us not only to calculate the enthalpy of mixing of the solid solution but also to tune its isobaric heat capacity as a function of temperature and chemical composition. This original DSC method to measure the enthalpy of formation of aluminium-based intermetallics (as well as the resulting enthalpy of mixing of this solid solution) is presented for the first time here. The temperature dependence of the Gibbs free energy of the metastable $Al_{13}(Fe,TM)_4$ (TM = Cr, Ni, Pt) solid solution components is obtained by means of the Kopp-Neumann rule [24]. To our knowledge this is the first time that a complete thermodynamic model for the $Al_{13}(Fe,TM)_4$ (with TM = Co, Cr, Ni, Pt) solid solution which accounts for both DFT simulations and DSC-based experimental data is proposed.

The case of the $Al_{13}(Fe,Mn)_4$ solid solution will be discussed in a forthcoming paper. This solid solution exhibits a relatively wide homogeneity range, which is particularly suited to formation enthalpy measurements by DSC. However, the solid solution is not complete and the energy of the $Al_{13}Mn_4$ reference state can only be determined by calculating its heat capacity. Therefore, the crystal chemistry of this solid solution will be investigated by combining 0 K DFT calculations with finite-temperature isobaric heat capacity calculations in order to perform its thermodynamic modelling.

2. Literature review on the $Al_{13}Fe_4$ intermetallic

The point group of the $Al_{13}Fe_4$ structure was first determined by Groth [25] based on morphological analysis, showing that the symmetry of this phase belongs to the monoclinic crystal system. Several authors have carried out further investigations using X-ray diffraction [26, 27, 28]. Their conclusions were not compatible with the morphological analysis carried out by Groth [25]. Indeed, they suggested an orthorhombic crystal structure since the X-ray analysis showed the presence of twofold axis. This contradiction was removed later by Black [29, 30] who developed a special Patterson method. Black showed that the reported twofold axis were induced by twinning in the structure, leading to an orthorhombic pseudo-symmetry. Thus, he solved the crystal structure leading to name this phase $Al_{13}Fe_4$ instead of Al_3Fe by reporting a monoclinic phase (C2/m space group) with 102 atomic sites per unit cell, 78 occupied by Al atoms and 24 occupied by Fe atoms. It was thus established that the $Al_{13}Fe_4$ structure is an isotype of the $Al_{13}Co_4$, $Al_{13}Rh_4$ and $Al_{13}Ru_4$ structures [31]. More recently, Grin et al. [21] refined the structure. According to the structure determination performed by Black [21, 29] and Grin et al. [21], the site occupation factors (sof) are almost all equal to one. Only one crystal site (site Al(2) using Grin• •'–ƒ–‹'• ˆ'" Žƒ––‹…‡ •‹–‡• t s exhibits partial occupation (0.7 for Al [21] and 0.92 for Al [29, 30]). The most recent single crystal structure determination performed by ‘ ’ « ‡ ˜ et al. [32] and Yanson et al. [33] show that all crystal sites of this structure are fully occupied. A crystallographic description of the $Al_{13}Fe_4$ structure including the crystallographic sites, their atomic coordinates and Wyckoff position is given in Table 1, following Grin et al. [21] notation for lattice sites.

Thermodynamic data are also available for this solid phase. The formation enthalpy of the $Al_{13}Fe_4$ phase was measured at 933 K by means of calorimetry [34, 35] and was calculated at 0 K using DFT simulations [36, 37, 38, 4]. The isobaric heat capacity was reported by several authors [39, 40, 41, 42], showing significantly lower values than the isobaric heat capacity obtained in the Kopp-Neumann approximation. More recent DFT investigations dedicated to the existence of vacancies in this structure have been carried out by Fang et al. [4]. Their calculations have shown that the addition of vacancies to the structure considerably reduces its thermodynamic stability.

Many phase diagram studies reporting solubility limits for this solid solution can be found in the literature. The solubility of the following elements in the $Al_{13}Fe_4$ has been investigated: TM = Co [43, 12], Cr [44, 12], Cu [45], Mn [12], Ni [46, 47, 12], Pt [17, 48], Ta [49], Ti [33], Zn [50]. The ternary solubility of the $Al_{13}Fe_4$ phase is generally limited, except in the case of the Al-Fe-Mn ternary system [51] as well as the Al-Fe-Co ternary system which exhibit a complete $Al_{13}Fe_4$-$Al_{13}Co_4$ solid solution.

3. Methodology

3.1. In-situ synthesis and enthalpy of formation measurement using DSC

The $Al_{13}Fe_{4-x}Co_x$ alloys were obtained from high purity metal powders (Al and Fe from Atlantic Equipment Engineers (3N purity) and Co from Sargent-Welch (3N purity)), mixed in a glass tube. The alloy compositions were chosen to match those of the solid solution end-members. The values of x (in $Al_{13}Fe_{4-x}Co_x$) therefore vary from 0 to 4 by 2/3 steps, leading to the synthesis of 7 different alloys. Note that the exact composition of the $Al_{13}Co_4$ binary intermetallic compound (isotype of $Al_{13}Fe_4$) deviates very slightly from this rule, in agreement with the measurements of Priputen et al. [52]. For the sake of simplification, we use the latter notation ($Al_{13}Fe_{4-x}Co_x$ with x=4) in this paper. The mass proportions were measured using a microbalance (uncertainty ±0.1mg). A mass of 20mg ± 0.5mg of this mixture is loaded into a lidded alumina crucible which is mounted on a Setaram Labsys Evo equipped with a type E DSC plate rod. A vacuum pump is then used to purge the air from the furnace chamber of the apparatus. After the air pressure is below 1 mbar, the furnace chamber is filled with high purity Ar (5N purity) to restore atmospheric pressure. This procedure is repeated a second time to ensure that the O_2 partial pressure is below about 10^{-6} atm before starting the experiment. A flow rate of 0.9 L/h of argon is applied and monitored throughout the thermal programme. Heating and cooling rate of 5 K/min is applied from room temperature up to 1073 K. The temperature and heat flow calibration of the DSC sensor is carried out prior to the measurements and verified after the measurements. Standard methods involving the measurement of melting temperature [53] and fusion enthalpy [54] of high-purity metal powders (3N purity) are used (Sn, Pb and Zn from Sigma Aldrich, Al from Atlantic Equipment Engineers). The resulting uncertainty is less than ±0.5 K for the temperature measurement and less than 1% for the heat flux. Note that the calibration procedure has been repeated each time the crucible is replaced.

High exothermic peak corresponding to the synthesis of the alloy was recorded during the temperature increase of each mixture, at 920 K ± 1 K. The weight losses were less than 1 wt.% after the synthesis. The samples were characterized following the synthesis by X-ray powder diffraction (XRD) at room temperature using a Malvern PanAlytical Empyrean 3 equipped with a graphite monochromator in the diffracted beam with Cu-Kα radiation. The diffractograms were also analysed with the Rietveld refinement technique. Table 2 summarizes the chemical composition, crystal structure and lattice parameter of the phase obtained from the Al-Fe-Co samples synthesized in the present work.

3.2. DFT calculations

The DFT calculations were conducted using the VASP code [55, 56] with pseudopotential and projector augmented wave (PAW) methods. A cutoff energy of 600 eV was determined for the plane wave basis set based on the convergence tests we performed. The calculations were done using the generalized gradient approximation (GGA) with the Perdew-Burke-Ernzerhof (PBE) exchange-correlation functional [57]. With respect to the magnetic state of Co, Cr, Fe and Ni, the calculations were performed with spin polarization. The relaxation of the lattice parameters as well as internal atomic positions have been carried out. The chosen convergence criterion is achieved for Hellman-Feynman forces less than 1 meV/Å. Finally, we used the linear tetrahedron method with Blöchl corrections to get very accurate total energy values [58]. We have calculated the total energy of all the end-members generated by distributing individual atoms in the five non-equivalent Fe sites, i.e.

considering the following SL model: $(Al)_{8}:(Fe,TM)_{1}:(Fe,TM)_{1}:(Fe,TM)_{1}:(Fe,TM)_{1}:(Fe,TM)_{8}$. This SL model generates 32 end-members for each ternary system. Dense grids of k-points (6 x 11 x 7) in the Brillouin zone were used. The formation enthalpy of each end-member is obtained by subtracting the calculated total energy to the molar fraction weighted sum of the energies of the pure elements in their Stable Element Reference (SER). The mixing enthalpy of the solid solution is then calculated by subtracting the formation enthalpy of the $Al_{13}Fe_{4-x}TM_{x}$ solid solution ($x \in$ 0, 4) to the molar fraction weighted sum of the formation enthalpy of reference compounds (i.e. $Al_{13}Fe_{4}$ and $Al_{13}TM_{4}$ pure compounds).

3.3. Thermodynamic modelling of the $Al_{13}Fe_{4-x}TM_{x}$ solid solution

The Gibbs free energy of a given phase can be computed at a finite temperature from 0 K DFT calculations of the formation enthalpies of all its end-members by means of the Bragg-Williams approximation [20] via the CEF: we consider the ideal configurational entropy on each site, neglecting the non-configurational entropy contributions as well as the interactions within sublattices. Only considering the 5 SLs related to the Fe sites, the Gibbs free energy of the $Al_{13}(Fe,TM)_{4}$ solid solution is expressed as:

$$G_m^{Al_{13}(Fe,TM)_4}(T) = {}^{ref}G_m^{Al_{13}(Fe,TM)_4}(T) + {}^{id}G_m^{Al_{13}(Fe,TM)_4}(T) \quad (1)$$

${}^{ref}G_m^{Al_{13}(Fe,TM)_4}$ is the Gibbs energy surface of reference which corresponds to the site occupancy weighted average molar Gibbs energies of the end-members

$$ {}^{ref}G_m^{Al_{13}(Fe,TM)_4}(T) = \sum_{i,j,k,l,m=Fe,TM} \left(y_i^{SL1}\, y_j^{SL2}\, y_k^{SL3}\, y_l^{SL4}\, y_m^{SL5}\right) \Delta H_{ijklm}^{Al_{13}(Fe,TM)_4} \quad (2)$$

y_j^{SLi} is the site occupancy of species j on the i-th SL, $\Delta H_{ijklm}^{Al_{13}(Fe,TM)_4}$ is the formation enthalpy of the end-member for which the first SL is occupied by element i, the second SL is occupied by element j etc... and the SL corresponding to the merging of all the Al sites is fully occupied by Al.

${}^{id}G_m^{Al_{13}(Fe,TM)_4}$ is the ideal Gibbs energy of mixing:

$$ {}^{id}G_m^{Al_{13}(Fe,TM)_4}(T) = -RT \sum_{i} a^{SL_i} \sum_{j=Fe,TM} y_j^{(i)} \ln y_j^{(i)} \quad (3)$$

R is the gas constant, a^{SL_i} is the multiplicity of the i-th SL. It should be noted that the configurational entropy is calculated for the entire structure. However, since the mixing is only allowed on the Fe sites, the contribution of the Al sites to the configurational entropy is null.

4. Results and Discussion

4.1. The $Al_{13}(Fe,Co)_4$ solid solution

4.1.1. Experimental results

The DSC heat-flow signals resulting from the in-situ synthesis of the $Al_{13}(Fe,Co)_4$ solid solution at different Co compositions are presented in Fig. 1. Table 3 reports the formation enthalpies of the $Al_{13}(Fe,Co)_4$ solid solution at 920 K obtained by integrating the exothermic DSC peaks shown in Fig. 1. From these results, the mixing enthalpy of the $Al_{13}(Fe,Co)_4$ solid solution at 920 K (references are $Al_{13}Fe_4$ and $Al_{13}Co_4$) has been calculated and plotted in Fig. 2.

4.1.2. DFT calculation and Finite-temperature calculation of site occupancy

Table 4 presents the DFT calculation of the total energy and formation enthalpy of the 32 end-members of the $Al_{13}(Fe,Co)_4$ solid solution. The mixing enthalpy of the $Al_{13}(Fe,Co)_4$ solid solution calculated by DFT (references are $Al_{13}Fe_4$ and $Al_{13}Co_4$) is reported in Fig. 3. Co sites occupancies have been calculated at 300 K and 1300 K respectively using our thermodynamic model as described in section 3.3. The results of these calculations are shown in Fig. 4 and Fig. 5. At last, the configurational entropy of the $Al_{13}(Fe,Co)_4$ solid solution has been computed from the DFT-calculated Co site occupancy and are compared to the configurational entropy of an ideal solution in Fig. 6.

4.1.3. Discussion

For the seven alloys synthesised in this work, the DSC signal shows a prominent and sharp exothermic peak, starting at 920 K. No other peaks are recorded at lower temperatures. We can thus conclude that the synthesis reaction of the intermetallic phase occurs at 920 K. Note that this synthesis temperature is lower than the one reported by Kubaschewski et al. [35] in direct reaction calorimetry (DRC) for the synthesis of the $Al_{13}Fe_4$ compound from high purity metal powders. Indeed, these authors reported a synthesis temperature of 933 K, the melting point of pure aluminium. However, it should be noted that the heat released by the formation reaction of the intermetallic compound leads to a very rapid increase of the sample temperature, which reaches 931 K ±1 K for the samples studied in this work. This makes it difficult to capture the onset of the reaction if numerical signal processing tools are not available. One should also note that the exothermic peak corresponding to the synthesis of our sample extends over a temperature range of about 22 K (from 909 K ±1 K to 931 K ±1 K). Strictly speaking, our measurements are not performed under isothermal conditions. However, the formation enthalpy variation over this temperature range is negligible. Indeed, this variation is equal to the difference between the integral of the heat capacity of the synthesized compound (C2/m structure) over this temperature range and the integral of the heat capacity obtained by the Kopp-Neumann approximation over this same temperature range. For the $Al_{13}Fe_4$ binary intermetallic compound we obtain a formation enthalpy variation of about 0.1 kJ/mol-at [39, 40, 41, 42], i.e. less than 0.5% of the lowest enthalpy of formation that we measured in this study. The XRD characterisation of each alloy was carried out after the DSC measurements and is summarised in Table 2. These results show that the conversion rate of the reactants into $Al_{13}(Fe,Co)_4$ solid solution is complete (above 99 wt.%). In fact, only sample # 2 contained some unmelted aluminium (2.9 wt.%). We have artificially removed this mass of unmelted aluminium in the formation enthalpy calculation. Note that our measurements of the formation enthalpy of the $Al_{13}Fe_4$ intermetallic compound are in good agreement with those performed by Kubaschewski et al. [35] and Biltz [34] as reported in Table 3. These measurements were also used to determine the mixing enthalpy of the solid solution, considering $Al_{13}Fe_4$ and $Al_{13}Co_4$ compounds as references. It appears in Fig. 2 that the enthalpy of mixing of this solid solution reflects an almost ideal behaviour at this temperature since the enthalpy values are relatively small (less than 1.8 kJ/mol in absolute values). Note that the formation enthalpy measurements reported in Table 3 all fall within ± 0.5 kJ/mol-at from the mean enthalpy value, for each alloy composition. We assume in this study that this range of ± 0.5 kJ/mol-at range is the confidence interval of our measurements. It results in a confidence interval of ± 1 kJ/mol-at for the mixing enthalpies calculated by summing the formation enthalpy values as reported in Figure 2.

Total energies and formation enthalpies of the 32 end-members of the solid solution are reported in Table 4. The formation enthalpy of the $Al_{13}Fe_4$ binary intermetallic compound calculated in this work (-31.335 kJ/mol) is in good agreement with calculations available in the literature (-31.840 kJ/mol [4], -33.481 kJ/mol [36], -30.876 kJ/mol [37], -31.840 kJ/mol [38]). To our knowledge, calculations or measurements of the thermodynamic parameters of any other end-members are not available in the literature. One should note that the spin polarisation calculations allowed us to confirm the results of Fang et al. [4] showing that the $Al_{13}Fe_4$ phase is non-magnetic. More generally, our calculations have shown that all the end-members considered in this study are non-magnetic.

The thermodynamic modelling of this solid solution was carried out according to the Calphad method. For this purpose, the formation enthalpy of each solid solution end-member calculated by DFT within this study were considered. Secondly, the isobaric heat capacities of all the solid solution end-members were slightly shifted towards those obtained by the Kopp-Neumann rule to fit the formation enthalpy measured at 920 K by DSC. Note that the isobaric heat capacity that we have optimised for the solid solution depends only on the chemical composition and temperature but not on configuration: all the end-members having an identical stoichiometry have an identical isobaric heat capacity. It should be noted that the heat capacity measurements of the $Al_{13}Fe_4$ binary compound available in the literature [39, 40, 41, 42] were not considered in this study. Indeed, these measurements were performed using conventional planar DSC which do not provide an accurate isobaric heat capacity measurement comparable to three-dimensional calorimetry methods associated with a specific calibration method [59, 60]. Consequently, the measurements performed by Illekova et al. [39], Zienert et al. [40] and Rank et al. [41, 42] are in strong contradiction with the formation enthalpy measurements and calculations available in the literature. Indeed, all the data available in the literature [4, 36, 37, 38, 34, 35] as well as our own calculations and measurements show that the formation enthalpy of the $Al_{13}Fe_4$ binary compound increases with temperature, indicating that its isobaric heat capacity is higher than the one obtained by the Kopp-Neumann rule. Note that this increase in formation enthalpy with temperature is also observed for all the solid solution end-members. Measurements provided by Illekova et al. [39], Zienert et al. [40] and Rank et al. [41, 42] show a strong opposite trend. We believe that the calculations and measurements of formation enthalpy available in the literature are more reliable and we must therefore discard the heat capacity measurements. At last, note that no interaction parameters were used. Our thermodynamic modelling results in the best possible compromise with all the experimental and calculated data considered. The optimised parameters show good agreement with our measurements and calculations (relative error less than 5%). The parameters we optimised are reported in Appendix.

Fig. 4 shows that the distribution of Co atoms on the different Fe sites of the $Al_{13}Fe_4$ structure is ordered at low temperature. The substitution of Fe atoms by Co atoms occurs preferentially on site Fe(1), and then on sites Fe(4), Fe(3), Fe(2) and Fe(5) when changing composition from $Al_{13}Fe_4$ to $Al_{13}Co_4$. These results agree with those of Pang et. al [12] indicating that Co preferentially occupies site Fe(1). Note however that the mixing enthalpy of the solid solution reported in Fig. 3 is relatively small (below 1 kJ/mol) which reflects a relatively low level of ordering at 0 K. Co site occupancies were computed at different temperatures from the Calphad modelling of the $Al_{13}(Fe,Co)_4$ solid solution we carried out in our work. In Fig. 4, the calculation of Co site occupancy at 300 K reveal that sites Fe(1), Fe(4), Fe(3) on the one hand, and sites Fe(2), Fe(5) on the other hand, have comparable Co occupancy values throughout the homogeneity range of the solid solution. Since the solid solution remains stable up to relatively high temperatures (more than 1300 K [43]), Co site occupancy were also computed at 1300 K as shown in Fig. 5. The five Fe sites are almost energetically equivalent at this temperature (i.e. exhibiting similar site occupancies). Finally, the configurational entropy of mixing of this solid solution presented in Fig. 6 allow us to quantify the level of ordering of the solid solution: While the solid solution remains partially ordered at 300 K, it is nearly completely disordered at 1300 K (the configurational entropy of mixing is almost identical to that of an ideal solid solution).

4.2. The $Al_{13}(Fe,Cr)_4$ solid solution

4.2.1. DFT calculation and Finite-temperature calculation of site occupancy

Table 5 presents the DFT calculation of the total energy and formation enthalpy of the 32 end-members of the $Al_{13}(Fe,Cr)_4$ solid solution. The mixing enthalpy of the $Al_{13}(Fe,Cr)_4$ solid solution calculated by DFT (references are $Al_{13}Fe_4$ and $Al_{13}Cr_4$) is reported in Fig. 7. Cr sites occupancies have been calculated at 1315 K as shown in Fig. 8. At last, the configurational entropy of the $Al_{13}(Fe,Co)_4$ solid solution has been computed from the DFT-calculated Cr site occupancy and compared to the ideal configurational entropy in Fig. 9.

4.2.2. Discussion

The example of the $Al_{13}(Fe,Cr)_4$ solid solution is quite particular. Indeed, as shown in Fig. 7, the ground-state of the solid solution consists of a single end-member referred as Fe:Fe:Fe:Fe:Cr (in addition to the intermetallic compounds of reference) reflecting the preferential substitution of Fe by Cr on site Fe(5). Moreover, note that the anti-structure Cr:Cr:Cr:Cr:Fe is one of the most unstable end-member. As a result, we should expect a strong Cr occupancy on site Fe(5). Our calculations are thus in good agreement with those of Pang et. al [12] showing that Cr preferentially occupies site Fe(5) of the $Al_{13}Fe_4$ structure. Other end-members are not stable at 0 K (formation energy higher than the calculated convex hull). The Cr site occupancies are presented at 1315 K in Fig. 8, the temperature at which the solid solution has the largest homogeneity range [61]. Site Fe(5) is the preferential site for Cr substitution throughout the homogeneity range of the solid solution, in good agreement with our 0 K DFT calculations. The other Fe sites (sites Fe(1), Fe(2), Fe(3) and Fe(4)) exhibit similar occupancy values. Finally, it should be noted that the configurational entropy calculations of Fig. 9 reveals that the solid solution is weakly ordered at 1315 K.

4.3. The $Al_{13}(Fe,Ni)_4$ solid solution

4.3.1. DFT calculation and Finite-temperature calculation of site occupancy

Table 6 presents the DFT calculations of the total energy and formation enthalpy of the 32 end-members of the $Al_{13}(Fe,Ni)_4$ solid solution. The mixing enthalpy of the $Al_{13}(Fe,Ni)_4$ solid solution calculated by DFT (references are $Al_{13}Fe_4$ and $Al_{13}Ni_4$) is reported in Fig. 10. Ni sites occupancies have been calculated at 300 K and 900 K as shown in Fig. 11 and Fig. 12. At last, the configurational entropy of the $Al_{13}(Fe,Ni)_4$ solid solution has been computed from the DFT-calculated Ni site occupancy and are compared to the ideal configurational entropy in Fig. 13.

4.3.2. Discussion

As shown in Fig. 10, Ni substitutes Fe on site Fe(4), and then on sites Fe(2), Fe(5), Fe(3) and Fe(1) when changing composition from $Al_{13}Fe_4$ to $Al_{13}Ni_4$. Interestingly, our calculations differ from those of Panget al. [12] suggesting that the substitution of Fe atoms by Ni atoms occurs preferentially on site Fe(1). Panget al. calculated that the energy difference between the structure with Ni substituted on site Fe(1) and Ni substituted on site Fe(4) to be 57.4 J/mol whereas our calculations show an energy difference between the two structures of 13 J/mol only. One could argue that such small energy differences imply that the two Fe sites are equivalent in terms of Ni substitution. However, this can only be valid for very low Ni concentrations since the calculations carried out by Panget al. only consider the substitution of a single Fe atom by a single Ni atom. In contrast, our calculations take into account the entire variation in chemical composition from $Al_{13}Fe_4$ to $Al_{13}Ni_4$. Ni site occupancies have also been computed at 900 K, temperature at which the solid solution extends the most [46]. Our calculations highlight that site Fe(1) alternatively switches from a very favourable site for Ni substitution at 900 K (if less than 5 % of the Fe atoms are substituted by Ni) to the least favourable site for Ni substitution (if more than 40 % of the Fe atoms are substituted by Ni) as reported in Fig 12. The situation appears even more contrasted when looking at our results presented in Fig. 11. Site Fe(1) is one of the least favourable one for substitution by Ni atoms while site Fe(4) is the most favourable one in almost the entire chemical composition range at 300 K. Therefore, our results show that chemical composition plays a crucial role in Ni site occupancy and that single atom substitution calculations may be too restrictive to conclude on the most favourable site for Ni occupancy. At last, note that the solid solution is relatively strongly ordered at 300 K but is close to ideal at 900 K as reported in Fig. 13.

4.4. The $Al_{13}(Fe,Pt)_4$ solid solution

4.4.1. DFT calculation and Finite-temperature calculation of site occupancy

Table 7 presents the DFT calculations of the total energy and formation enthalpy of the 32 end-members of the $Al_{13}(Fe,Pt)_4$ solid solution. The mixing enthalpy of the $Al_{13}(Fe,Pt)_4$ solid solution calculated by DFT (references are $Al_{13}Fe_4$ and $Al_{13}Pt_4$) is reported in Fig. 14. Pt sites occupancies have been calculated at 300 K and 1373 K as shown in Fig. 15 and Fig. 16. At last, the configurational entropy of the $Al_{13}(Fe,Pt)_4$ solid solution has been computed from the DFT-calculated Pt site occupancy and are compared to the ideal configurational entropy in Fig. 17.

4.4.2. Discussion

The calculated 0 K mixing enthalpy reported in Fig. 14 indicates that the substitution of Fe atoms by Pt atoms occurs successively on sites Fe(1), Fe(4), Fe(5), Fe(2) and Fe(3). Our results therefore show that the preferred site for Pt occupancy is site Fe(1) in good agreement with investigations carried out by Yamada et. al [17]. One should also note that this pseudo-binary solid solution is rather stable (i.e. large negative enthalpy of mixing) suggesting a relatively strong level of ordering compared to the other studied solid solutions. Pt site occupancies computed at 300 K (Fig. 15) show both the substitution sequence identified in Fig. 14 and the strong ordering of the solid solution since the Fe sites all have very different occupancy values. The Pt site occupancies were also computed at 1373 K as reported in Fig. 16, temperature at which the solid solution extends the most [48]. One should notice that sites Fe(5) and Fe(2) are the only ones that can be considered as equivalent at this temperature. Configurational entropy of mixing computed at 300 K and 1373 K (Fig. 17) clearly indicates that the solid solution remains strongly ordered.

5. Discussion

As explained in the introduction, the design of a SL model for a given solid solution in the framework of the CEF can be achieved after a careful analysis of the crystal structure and the identification of the origin the non-stoichiometry via its crystal chemistry. The solution model must allow to accurately describe the configurational entropy of mixing at high temperature in the homogeneity range of the phase and to a lesser extent, outside the homogeneity range if one wants to accurately describe its metastable behaviour. Moreover, since the number of end-members increases exponentially with the number of SL, a SL model must also result from a compromise between the precision of the description of the crystal structure and the simplicity of use of the model, which suggests a reduction in the number of SL if possible. The examples considered in this paper clearly show that the $Al_{13}(Fe,Co)_4$ and $Al_{13}(Fe,Ni)_4$ solid solutions are almost completely disordered at 1373 K and 900 K, respectively, and can be considered ideal. For these two solid solutions, it is therefore recommended to merge all Fe sites of the $Al_{13}Fe_4$ structure into a single SL.

The $Al_{13}(Fe,Cr)_4$ solid solution is slightly different. Cr occupancy values on site Fe(5) remain significantly different than those of all the other Fe sites, up to 1315 K. Despite this, the configurational entropy we have calculated is relatively close to that of an ideal solution, showing weak ordering at 1315 K. This is due to the comparable Cr occupancy values on sites Fe(1) to Fe(4) reflecting the disordered nature of the solid solution. It should also be noted that the multiplicity of site Fe(5) is three times lower than the combined multiplicity of sites Fe(1) to Fe(4); the ordering observed on site Fe(5) thus has a moderate impact on the configurational entropy of the solid solution. Therefore, for simplicity purposes, we consider that merging all Fe sites into a single SL is acceptable.

On the contrary, the $Al_{13}(Fe,Pt)_4$ solid solution remains ordered, over a wide temperature range from 300 K to 1373 K. The Pt occupancy values show that only sites Fe(2) and Fe(5) can be considered as equivalent at 1373 K. The calculation of the configurational entropy of mixing shows the inability of a single SL model for the Fe sites to accurately describe the thermodynamic behaviour of this solid solution. A simplified SL model for Fe sites could still be considered if one is only interested in the thermodynamic stability of the solid solution, and not in its metastability. For this purpose, site Fe(1) should be accounted for by one SL while all the other Fe sites can be combined in a second SL since their occupancy values are comparable in the solid solution homogeneity range, as shown in Fig. 16. This is only acceptable because the homogeneity range of the solid solution is particularly limited, as reported by Grushko [48] and shown in the Fig. 14 to 17. However, this is not what we recommend in the present paper. A reliable thermodynamic modelling of this solid solution should be based on a 4-SL model for the Fe sites: one SL for sites Fe(2) and Fe(5) and one SL for each remaining Fe site.

In order to design an optimal SL model for the $Al_{13}(Fe,TM)_4$ solid solution, the potential presence of structural vacancies in the $Al_{13}Fe_4$ structure has to be analysed. As mentioned in section 2, the reported values for *sof* of site Al(2) in the $Al_{13}Fe_4$ structure differs depending on the studies available in the literature. Some studies reported a partial occupancy of the site Al(2) (*sof* of 0.7 [29, 30] and 0.92 [21]) while others have shown that the site Al(2) is fully occupied. According to our literature review, the most reliable structure determination is presented in the work of ‘ ’ « ‡ ˜ *et al.* [32]. These authors found no vacancy defects in this crystal structure. This is fully consistent with the DFT calculations performed by Fang *et al.* [4] which showed that the presence of vacancies in the structure is energetically highly unfavourable. It should be noted that partial site occupancy was not reported for either the isotypic $Al_{13}Ru_4$ structure [21] or the partially disordered $Al_{13}Fe_4$ structure containing 5.5 at.% of Ti as presented by Yanson *et al.* [33]. In this context, the partial occupancy of this crystal site must be questioned. The *sof* value of 0.7 [29, 30] and 0.92 [21] are equivalent to a deficit of 16 and 4 electrons per unit cell respectively over the 1638 electrons of the ideal structure. These very small differences in electronic densities appear to be measurement artifacts, which could also explain why the partial occupancy values reported by Black [29, 30] and Grin *et al.* [21] are so different from each other. According to all these observations and results, SL models that include structural vacancies are not recommended for the thermodynamic modelling of the $Al_{13}(Fe,TM)_4$ solid solution. This is in contrast with the CEF model developed by Sundman *et al.* [22] which has been extensively used in the past years [22, 62, 63, 64, 65, 66, 67].

As a final remark, it should be noted that in most cases, the solubility of an element in the $Al_{13}Fe_4$ binary compound usually involves substitutions on the Fe sites. In fact, only the following elements substitute on Al sites: 1) Ta [49], 2) Ti [68], 3) Si [69] and 4) Zn [50]. Furthermore, the solid solutions obtained with these elements show particularly limited homogeneity ranges [49, 68, 70, 50], compared to those for which Fe atoms are substituted. Therefore, the SL model developed by Fang *et al.* [4] seems to be unsuitable for modelling these solid solutions. Indeed, in this model, all Fe sites have been combined in a single SL and the Al sites have been distinguished. Moreover, the authors suggested to split sites Al(5), Al(7) and Al(9) and to merge the remaining Al sites. However, the same authors have shown that Si can substitute Al on sites Al(8) and Al(9) [69], which cannot be described by their SL model. Similarly, XRD analysis carried out by Yanson *et al.* [33] showed that Ti substitutes Al on sites Al(9), Al(10), Al(11) and Al(15), which cannot be correctly described with the latter model. In addition, the SL-model proposed by Fang *et al.* was designed by calculating structures with a single atom substituted. We have shown in this paper that this procedure can sometimes lead to erroneous conclusions regarding the preferential substitution sites of solid solutions. We thus believe that this model is well suited to describe the thermodynamic behaviour of the $Al_{13}Fe_4$ compound in the Al-Fe binary system but can hardly be used for higher order systems.

6. Conclusion and perspectives

We presented in this work an original method to define an optimal SL model for the $Al_{13}(Fe,TM)_4$ multicomponent solid solution along with its precise parameterisation *via* the Calphad approach. It was experimentally confirmed that the complete solid solution in the $Al_{13}Fe_4$-$Al_{13}Co_4$ pseudo-binary section is associated with a virtually null enthalpy of mixing. Our novel *in-situ* synthesis of this solid solution for distinct compositions, starting from pure elemental powders, provided precise enthalpy of formation data at 920 K when compared to the literature, *i.e.*, -26.8 kJ/mol-at for $Al_{13}Fe_4$ binary compound *versus* -27.9 kJ/mol-at [34] and -26.2 kJ/mol-at [35]. These data were then used not only to calculate the enthalpy of mixing of this pseudo-binary section but also to parametrise the Gibbs free energy of the solid solution end-members.

Our approach allowed us to explore the crystal chemistry of the solid solutions by computing the TM site occupancy on the Fe crystal sites as a function of temperature using the thermodynamic model built in this work. The ordering of the solid solution was also quantified as function of temperature. It was found that some chemical ordering exists for different pseudo-binary sections at low temperature because of the stability of some end-members which have large and negative enthalpy of formation (especially for Pt and Ni). It is interesting to note that even though large enthalpy of formation were calculated for both $Al_{13}Pt_4$ (-49.9 kJ/mol-at) and $Al_{13}Ni_4$ (-31.1 kJ/mol-at), they would not form at equilibrium at low temperature as the equilibrium phase assemblage in these systems leads to even lower enthalpy of formation, i.e. -64.5 kJ/mol-at for the ($Al_{21}Pt_5$ + $Al_{21}Pt_8$) phase assemblage for the Al-Pt system [71] and -45.2 kJ/mol-at for the (fcc+Al_3Ni-$D0_{11}$) phase assemblage for the Al-Ni system [72]. At higher temperature, the virtually-zero enthalpy of mixing for the $Al_{13}(Fe,TM)_4$ solid solutions (TM = Co, Cr, Ni) leads to almost ideal configurational entropy of mixing values.

As a conclusion, a 2-SL model (one SL resulting from the merging the Al sites, one SL resulting from the merging of the Fe sites of the $Al_{13}Fe_4$ structure) seems well suited for describing the $Al_{13}(Fe,TM)_4$ solid solutions (TM = Co, Cr, Ni). In contrast, the $Al_{13}(Fe,Pt)_4$ solid solution has to be described using a 5-SL model (four SL for the Fe sites, one SL for the Al sites).

The next steps to improve the precision of our methodology are 1) to directly measure the heat capacity of key stable solid solution compositions using a 3D-Cp Pt rod [73] and 2) to complement our DFT calculations at 0 K by building the temperature dependency of the Gibbs free energy using a quasi-harmonic-based method involving the evaluation of either the elastic constants or the phonon spectrum of a given crystal structure [74].

7. Acknowledgement

We acknowledge the support of the Natural Sciences and Engineering Research Council of Canada (NSERC) via the Discovery Grant of Prof. Harvey (RGPIN-2017-06168).

We acknowledge the support of Alliance Grants (ALLRP 560998-r ‡•–‹–Ž‡† ó Š‡”•‘†›•ƒ•‹… ƒ•† physi… ƒŽ ’”‘’‡”–› •‘†‡Ž• ˆ‘” –Š‡ ’”‘†—…–‹‘• ‘ˆ ‰”‡‡•‡” ƒŽ—•‹•—• ƒŽŽ‘›•ó

Calcul Quebec and Calcul Canada are thanked for providing the calculation tools.

Daniel Chartrand and Thierry Maris are acknowledged for their work on XRD analysis.

References

[1] L. Zhang, J. Gao, L. N. W. Damoah, D. G. Robertson, Mineral Processing and Extractive Metallurgy Review 33 (2012) 99 157.

[2] S. K. Das, Materials Science Forum 519 (2006) 1239 1244.

[3] Z. Que, Y. Wang, Z. Fan, Metallurgical and Materials Transactions A 49 (2018) 2173 2181.

[4] C. Fang, A. Dinsdale, Z. Que, Z. Fan, Journal of Physics: Materials 2 (2019) 015004.

[5] P. R. Goulart, J. E. Spinelli, N. Cheung, A. Garcia, Materials Chemistry and Physics 119 (2010) 272 278.

[6] D. Liang, P. Korgul, H. Jones, Acta materialia 44 (1996) 2990 3004.

[7] J. Mathew, G. Remy, M. A. Williams, F. Tang, P. Srirangam, JOM 71 (2019) 4362 4369.

[8] ä ƒ•á ä —•ƒ”á ä …•ƒ›á ä ï ‡‹ŽŽ›á •‡‡ƒ–ƒŽ ƒ‰ƒœ‹•‡ ... 202 206.

[9] M. M. Pariona, V. Teleginski, K. dos Santos, S. Machado, A. J. Zara, N. K. Zurba, R. Riva, Surface and Coatings Technology 206 (2012) 2293 2301.

[10] J. Wang, Y. Zhou, M. He, L. Xu, P. Wangyang, Journal of Alloys and Compounds 717 (2018) 14 20.

[11] A. Samuel, G. Garza-Elizondo, H. Doty, F. Samuel, Materials & Design 80 (2015) 99 108.

[12] N. Pang, Z. Shi, C. Wang, N. Li, Y. Lin, Materials 14 (2021) 768.

[13] W. Zheng, H. Mao, X.-G. Lu, Y. He, L. Li, M. Selleby, J. Ågren, Journal of Alloys and Compounds 742 (2018) 1046 1057.

[14] J. R. Davis, Alloying: Understanding the Basics, ASM international, 2001.

[15] M. ‘ † ³ ” ‘ ˜, ž P. Novák, I. Marek, D. Vojtech, in: Key Engineering Materials, volume 592, Trans Tech Publ, pp. 639 642.

[16] M. V. Canté, C. Brito, J. E. Spinelli, A. Garcia, Materials & Design 51 (2013) 342 346.

[17] T. Yamada, T. Kojima, E. Abe, S. Kameoka, Y. Murakami, P. Gille, A. P. Tsai, Journal of the American Chemical Society 140 (2018) 3838 3841.

[18] M. Armbrüster, K. Kovnir, M. Friedrich, D. Teschner, G. Wowsnick, M. Hahne, P. Gille, L. Szentmiklósi, M. Feuerbacher, M. Heggen, et al., Nature materials 11 (2012) 690 693.

[19] H. Lukas, S. G. Fries, B. Sundman, Computational thermodynamics: the Calphad method, Cambridge university press, 2007.

[20] M. Hillert, Journal of Alloys and Compounds 320 (2001) 161 176.

[21] J. Grin, U. Burkhardt, M. Ellner, K. Peters, Zeitschrift für Kristallographie-Crystalline Materials 209 (1994) 479 487.

[22] B. Sundman, I. Ohnuma, N. Dupin, U. R. Kattner, S. G. Fries, Acta Materialia 57 (2009) 2896 2908.

[23] W. L. Bragg, E. J. Williams, Proceedings of the Royal Society of London. Series A, Containing Papers of a Mathematical and Physical Character 145 (1934) 699 730.

[24] H. Kopp, Philosophical Transactions of the Royal Society of London (1865) 71–202.

[25] P. Groth, Leipzig: Verlag von Wilhelm Engelmann (1906).

[26] E. Bachmetew, Zeitschrift für Kristallographie-Crystalline Materials 89 (1934) 575–586.

[27] A. Osawa, Sci. Rep. Tohoku Univ 22 (1933) 803–823.

[28] G. Phragmén, Journal of the Institute of Metals 77 (1950) 489–551.

[29] P. Black, Acta Crystallographica 8 (1955) 43–48.

[30] P. Black, Acta Crystallographica 8 (1955) 175–182.

[31] P. Scheid, C. Chatelier, J. Ledieu, V. Fournée, E. Gaudry, Acta Crystallographica Section A: Foundations and Advances 75 (2019) 314–324.

[32] P. ‘ ’ « ‡ ˜ ‹ ‚ A. Smontara, J. Ivkov, M. Wencka, M. Komelj, P. ‰ Š ‹ « Vrtnik, M. Bobnar, Z. ƒ ‰ Ž ‹ « ‹ © B. Bauer, et al., Physical Review B 81 (2010) 184203.

[33] T. Yanson, N. Manyako, O. Bodak, R. Cêrny, R. Gladyshevskii, K. Yvon, Journal of Alloys and Compounds 219 (1995) 135–138.

[34] W. Biltz, Zeitschrift für Metallkunde 29 (1937) 72–79.

[35] O. Kubaschewski, W. Dench, Acta Metallurgica 3 (1955) 339–346.

[36] M. Mihalkovi«, M. Widom, Physical Review B 85 (2012) 014113.

[37] A. Van der Kraan, K. Buschow, Physica B+ C 138 (1986) 61–65.

[38] T. Klaver, G. Madsen, R. Drautz, Intermetallics 31 (2012) 137–144.

[39] E. Illeková, J.-C. Gachon, J.-J. Kuntz, in: Thermophysics 2002. Meeting of the Thermophysical Society Working Group of the Slovak Physical Society, October 24-25, 2002, K«ice, Slovakia, pp. 71–76.

[40] T. Zienert, A. Leineweber, O. Fabrichnaya, Journal of Alloys and Compounds 725 (2017) 848–859.

[41] M. Rank, P. Gotcu, P. Franke, H. J. Seifert, Intermetallics 94 (2018) 37 23.

[42] M. Rank, P. Franke, H. J. Seifert, International Journal of Materials Research 110 (2019) 406 421.

[43] L. Zhu, S. Soto-Medina, R. G. Hennig, M. V. Manuel, Journal of Alloys and Compounds 815 (2020) 152110.

[44] B. Bauer, P. Gille, Zeitschrift für anorganische und allgemeine Chemie 637 (2011) 2052 2058.

[45] C. Liu, C. Fan, IUCrData 3 (2018) x180363.

[46] L. Zhang, Y. Du, Calphad 31 (2007) 529 540.

[47] L. Zhang, Y. Du, H. Xu, C. Tang, H. Chen, W. Zhang, Journal of alloys and compounds 454 (2008) 129 135.

[48] B. Grushko, Journal of Alloys and Compounds 829 (2020) 154444.

[49] V. Witusiewicz, A. Bondar, U. Hecht, V. Voblikov, N. Tsyganenko, O. Fomichov, M. Karpets, V. Petyukh, T. Y. Velikanova, Journal of Materials Science 48 (2013) 3712.

[50] I. Lee, K. Han, I. Ohnuma, R. Kainuma, Journal of Alloys and Compounds 854 (2021) 157163.

[51] S. Balanetskyy, D. Pavlyuchkov, T. Velikanova, B. Grushko, Journal of Alloys and Compounds 619 (2015) 211 220.

[52] P. Priputen, M. Kusý, M. Drienovský, D. [illegible] Janovec, Journal of Alloys and Compounds 647 (2015) 486 497.

[53] ASTM-E967-18, ASTM International, West Conshohocken, PA (2018).

[54] ASTM-E968-02, ASTM International, West Conshohocken, PA (2014).

[55] G. Kresse, J. Furthmüller, Physical review B 54 (1996) 11169.

[56] G. Kresse, D. Joubert, Physical review b 59 (1999) 1758.

[57] J. P. Perdew, K. Burke, M. Ernzerhof, Physical review letters 77 (1996) 3865.

[58] P. E. Blöchl, Physical review B 50 (1994) 17953.

[59] E. Calvet, H. Prat, Récents progrès en microcalorimétrie, volume 6, Dunod, 1958.

[60] C. N. de Castro, M. Lourenço, M. Sampaio, Thermochimica Acta 347 (2000) 85–91.

[61] D. Pavlyuchkov, B. Przepiórzyński, W. Kowalski, T. Y. Velikanova, B. Grushko, Calphad 45 (2014) 194–203.

[62] M. Ostrowska, G. Cacciamani, Journal of Alloys and Compounds 794 (2019) 553–568.

[63] M. Noori, B. Hallstedt, Calphad 74 (2021) 102288.

[64] T. Zienert, O. Fabrichnaya, Journal of Alloys and Compounds 743 (2018) 795–811.

[65] M. H. Jacobs, R. Schmid-Fetzer, Calphad 33 (2009) 170–178.

[66] A. T. Phan, M.-K. Paek, Y.-B. Kang, Acta Materialia 79 (2014) 1–15.

[67] W. Zheng, S. He, M. Selleby, Y. He, L. Li, X.-G. Lu, J. Ågren, Calphad 58 (2017) 34–49.

[68] M. Palm, J. Lacaze, Intermetallics 14 (2006) 1291–1303.

[69] C. Fang, Z. Que, A. Dinsdale, Z. Fan, Intermetallics 126 (2020) 106939.

[70] M. C. Marker, B. Skolyszewska-Kühberger, H. S. Effenberger, C. Schmetterer, K. W. Richter, Intermetallics 19 (2011) 1919–1929.

[71] D. Kim, Z.-K. Liu, V. Manga, S. Prins, et al. (2013).

[72] N. Dupin, I. Ansara, B. Sundman, Calphad 25 (2001) 279–298.

[73] G. Boissonnet, G. Bonnet, F. Pedraza, Journal of Materials and Applications 8 (2019) 59–64.

[74] S.-L. Shang, Y. Wang, D. Kim, Z.-K. Liu, Computational Materials Science 47 (2010) 1040–1048.

8. Table caption

Table 1: Crystallographic description of the $Al_{13}Fe_4$ • – ” — … – — ” ‡ ƒ … … ‘ ” † ‹ • ‰ – ‘ ” ‹ • ï • • ‘ – ƒ – ‹ ‘ • t s ä

Site	Wyckoff position	x	y	z
Fe(1)	4i	0.0851	0	0.3821
Fe(2)	4i	0.4018	0	0.6234
Fe(3)	4i	0.0906	0	0.9889
Fe(4)	4i	0.4031	0	0.9859
Fe(5)	8j	0.3195	0.2938	0.2777
Al(1)	4i	0.0649	0	0.1743
Al(2)	4i	0.3232	0	0.2819
Al(3)	4i	0.2377	0	0.5349
Al(4)	4i	0.0736	0	0.5803
Al(5)	4i	0.2406	0	0.9608
Al(6)	4i	0.4792	0	0.8288
Al(7)	2d	0.5	0	0.5
Al(8)	4i	0.3057	0	0.7728
Al(9)	4i	0.087	0	0.7885
Al(10)	8j	0.185	0.2168	0.1106
Al(11)	8j	0.3677	0.2113	0.1097
Al(12)	8j	0.1783	0.221	0.3346
Al(13)	8j	0.4916	0.2334	0.3296
Al(14)	8j	0.3634	0.2188	0.4786
Al(15)	4g	0	0.2496	0

Table 2: Chemical composition and Rietveld refinement from XRD characterisation of the Al-Fe-Co samples.

Sample number	Nominal composition	Space group	Phase wt.%	Lattice parameters Å and °			
	x (in $Al_{13}Fe_{4-x}Co_{x}$)			a	b	c	t
1	0	C2/m	99.9	15.5039(6)	8.0725(1)	12.4705(2)	107.6958(3)
2	2/3	C2/m	97.1	15.4682(7)	8.0869(4)	12.4636(3)	107.722(1)
3	4/3	C2/m	100	15.4194(4)	8.1024(2)	12.4486(3)	107.8168(4)
4	6/3	C2/m	100	15.3615(5)	8.1250(3)	12.4259(4)	107.8446(6)
5	8/3	C2/m	100	15.3176(4)	8.1291(2)	12.4142(5)	107.8964(8)
6	10/3	C2/m	100	15.2300(5)	8.1528(2)	12.3972(4)	107.9934(6)
7	4	C2/m	99.3	15.1722(5)	8.1081(2)	12.3512(4)	107.8474(6)

Table 3: ‘ ” • ƒ – ‹ ‘ • ‡ • – Š ƒ Ž ¿H_f of the $Al_{13}(Fe,Co)_4$ solid solution measured at 920 K compared to literature data. Reference states are Al (fcc), Fe (bcc) and Co (bcc) pure elements

Composition x (in $Al_{13}Fe_{4-x}Co_{x}$)	¿H_f kJ/mol- at				Method	Ref.
	run1	run2	run3	Average		
0	-26.71	-26.84	-26.73	-26.76	DSC	This work
				-27.9	DRC at 933 K	[34]
				-26.2	Solution calorimetry	[35]
2/3	-28.14	-27.27	-27.86	-27.76	DSC	This work
4/3	-29.55	-28.75	-29.28	-29.19	DSC	This work
6/3	-28.71	-28.00	-28.56	-28.42	DSC	This work
8/3	-30.16	-29.91	-29.36	-29.81	DSC	This work
10/3	-31.03	-31.07	-30.89	-31.00	DSC	This work
4	-32.29	-32.71	-32.59	-32.53	DSC	This work

Table 4: First-principle calculation of the end-members in the $Al_{13}(Fe,Co)_4$ • ' Ž ‹ † • ' Ž — – ‹ ' • ƒ notation ” ‹ • ï • for lattice sites is adopted [21]. E_{tot} is the total energies of the end-members, ΔH_f is the formation enthalpies of the end-members. Reference states are Al (fcc), Fe (bcc) and Co (hcp) pure elements.

Site multiplicity					E_{tot} eV	ΔH_f kJ/mol- at
Fe(1) 4	Fe(2) 4	Fe(3) 4	Fe(4) 4	Fe(5) 8		
Fe	Fe	Fe	Fe	Fe	-523.519	-31.335
Co	Co	Co	Co	Co	-500.337	-37.147
Co	Fe	Fe	Fe	Fe	-520.169	-32.800
Fe	Co	Fe	Fe	Fe	-520.044	-32.681
Fe	Fe	Co	Fe	Fe	-520.005	-32.644
Fe	Fe	Fe	Co	Fe	-520.139	-32.772
Co	Co	Fe	Fe	Fe	-516.449	-33.885
Co	Fe	Co	Fe	Fe	-516.597	-34.025
Co	Fe	Fe	Co	Fe	-516.638	-34.064
Fe	Fe	Fe	Fe	Co	-515.819	-33.289
Fe	Co	Co	Fe	Fe	-516.369	-33.810
Fe	Co	Fe	Co	Fe	-516.562	-33.993
Fe	Fe	Co	Co	Fe	-516.544	-33.976
Co	Fe	Fe	Fe	Co	-512.168	-34.468
Co	Co	Co	Fe	Fe	-512.669	-34.942
Fe	Co	Fe	Fe	Co	-512.188	-34.488
Co	Co	Fe	Co	Fe	-512.732	-35.002
Fe	Fe	Co	Fe	Co	-512.201	-34.499
Co	Fe	Co	Co	Fe	-512.883	-35.145
Fe	Fe	Fe	Co	Co	-512.272	-34.566
Fe	Co	Co	Co	Fe	-512.712	-34.983
Co	Co	Fe	Fe	Co	-508.246	-35.391
Co	Fe	Co	Fe	Co	-508.400	-35.537
Fe	Co	Co	Fe	Co	-508.421	-35.556
Co	Fe	Fe	Co	Co	-508.451	-35.585
Co	Co	Co	Co	Fe	-508.751	-35.868
Fe	Co	Fe	Co	Co	-508.478	-35.610
Fe	Fe	Co	Co	Co	-508.466	-35.599
Co	Co	Co	Fe	Co	-504.331	-36.292
Co	Co	Fe	Co	Co	-504.400	-36.358
Co	Fe	Co	Co	Co	-504.521	-36.472
Fe	Co	Co	Co	Co	-504.542	-36.491

Table 5: First-principle calculation of the end-members in the $Al_{13}(Fe,Cr)_4$ • ' Ž ‹ † • ' Ž — – ‹ ' • ƒ – r ä " ‹ • ï • • ' – ƒ – ‹ ' • for lattice sites is adopted [21]. E_{tot} is the total energies of the end-members, ÃH_f is the formation enthalpies of the end-members. Reference states are Al (fcc), Fe (bcc) and Cr (bcc) pure elements

Site multiplicity					E_{tot} eV	¿H_f kJ/mol- at
Fe(1) 4	Fe(2) 4	Fe(3) 4	Fe(4) 4	Fe(5) 8		
Fe	Fe	Fe	Fe	Fe	-523.519	-31.335
Cr	Cr	Cr	Cr	Cr	-531.483	-10.134
Cr	Fe	Fe	Fe	Fe	-523.574	-26.589
Fe	Cr	Fe	Fe	Fe	-523.065	-26.107
Fe	Fe	Cr	Fe	Fe	-524.583	-27.543
Fe	Fe	Fe	Cr	Fe	-524.385	-27.356
Cr	Cr	Fe	Fe	Fe	-524.870	-23.045
Cr	Fe	Cr	Fe	Fe	-524.561	-22.753
Cr	Fe	Fe	Cr	Fe	-524.741	-22.923
Fe	Fe	Fe	Fe	Cr	-527.199	-25.248
Fe	Cr	Cr	Fe	Fe	-524.932	-23.104
Fe	Cr	Fe	Cr	Fe	-524.440	-22.638
Fe	Fe	Cr	Cr	Fe	-525.465	-23.607
Cr	Fe	Fe	Fe	Cr	-527.705	-20.927
Cr	Cr	Cr	Fe	Fe	-525.939	-19.257
Fe	Cr	Fe	Fe	Cr	-527.952	-21.161
Cr	Cr	Fe	Cr	Fe	-525.837	-19.161
Fe	Fe	Cr	Fe	Cr	-527.990	-21.198
Cr	Fe	Cr	Cr	Fe	-525.732	-19.062
Fe	Fe	Fe	Cr	Cr	-528.340	-21.529
Fe	Cr	Cr	Cr	Fe	-525.811	-19.137
Cr	Cr	Fe	Fe	Cr	-529.092	-17.441
Cr	Fe	Cr	Fe	Cr	-528.401	-16.787
Fe	Cr	Cr	Fe	Cr	-528.843	-17.206
Cr	Fe	Fe	Cr	Cr	-528.814	-17.178
Cr	Cr	Cr	Cr	Fe	-527.187	-15.639
Fe	Cr	Fe	Cr	Cr	-528.798	-17.163
Fe	Fe	Cr	Cr	Cr	-529.150	-17.496
Cr	Cr	Cr	Fe	Cr	-530.042	-13.570
Cr	Cr	Fe	Cr	Cr	-530.092	-13.617
Cr	Fe	Cr	Cr	Cr	-529.879	-13.415
Fe	Cr	Cr	Cr	Cr	-530.150	-13.672

Table 6: First-principle calculation of the end-members in the $Al_{13}(Fe,Ni)_4$ solid •'Ž——‹'• ƒ– r ä ”‹•ï• notation for lattice sites is adopted [21]. E_{tot} is the total energies of the end-members, ΔH_f is the formation enthalpies of the end-members. Reference states are Al (fcc), Fe (bcc) and Ni (fcc) pure elements.

Site multiplicity					E_{tot} eV	ΔH_f kJ/mol- at
Fe(1) 4	Fe(2) 4	Fe(3) 4	Fe(4) 4	Fe(5) 8		
Fe	Fe	Fe	Fe	Fe	-523.519	-31.335
Ni	Ni	Ni	Ni	Ni	-456.291	-31.081
Ni	Fe	Fe	Fe	Fe	-513.679	-32.606
Fe	Ni	Fe	Fe	Fe	-513.236	-32.186
Fe	Fe	Ni	Fe	Fe	-513.512	-32.447
Fe	Fe	Fe	Ni	Fe	-513.694	-32.619
Ni	Ni	Fe	Fe	Fe	-502.129	-32.194
Ni	Fe	Ni	Fe	Fe	-503.001	-33.019
Ni	Fe	Fe	Ni	Fe	-502.964	-32.984
Fe	Fe	Fe	Fe	Ni	-501.890	-31.968
Fe	Ni	Ni	Fe	Fe	-502.481	-32.527
Fe	Ni	Fe	Ni	Fe	-502.733	-33.058
Fe	Fe	Ni	Ni	Fe	-502.630	-32.668
Ni	Fe	Fe	Fe	Ni	-490.699	-31.959
Ni	Ni	Ni	Fe	Fe	-490.835	-32.088
Fe	Ni	Fe	Fe	Ni	-491.161	-32.397
Ni	Ni	Fe	Ni	Fe	-491.109	-32.348
Fe	Fe	Ni	Fe	Ni	-491.174	-32.408
Ni	Fe	Ni	Ni	Fe	-491.364	-32.588
Fe	Fe	Fe	Ni	Ni	-491.360	-32.585
Fe	Ni	Ni	Ni	Fe	-491.224	-32.456
Ni	Ni	Fe	Fe	Ni	-479.184	-31.644
Ni	Fe	Ni	Fe	Ni	-479.792	-32.219
Fe	Ni	Ni	Fe	Ni	-480.142	-32.550
Ni	Fe	Fe	Ni	Ni	-479.705	-32.137
Ni	Ni	Ni	Ni	Fe	-479.259	-31.715
Fe	Ni	Fe	Ni	Ni	-480.310	-32.710
Fe	Fe	Ni	Ni	Ni	-479.764	-32.193
Ni	Ni	Ni	Fe	Ni	-468.102	-31.676
Ni	Ni	Fe	Ni	Ni	-468.067	-31.643
Ni	Fe	Ni	Ni	Ni	-468.130	-31.702
Fe	Ni	Ni	Ni	Ni	-468.370	-31.929

Table 7: First-principle calculation of the end-members in the $Al_{13}(Fe,Pt)_4$ • ' Ž ‹ † • ' Ž — – ‹ ' • ƒ – r ä " ‹ • ï • notation for lattice sites is adopted [21]. E_{tot} is the total energies of the end-members, ÃH_f is the formation enthalpies of the end-members. Reference states are Al (fcc), Fe (bcc) and Pt (fcc) pure elements.

Site multiplicity					E_{tot} eV	¿H_f kJ/mol- at
Fe(1) 4	Fe(2) 4	Fe(3) 4	Fe(4) 4	Fe(5) 8		
Fe	Fe	Fe	Fe	Fe	-523.519	-31.335
Pt	Pt	Pt	Pt	Pt	-491.286	-49.872
Pt	Fe	Fe	Fe	Fe	-520.748	-36.902
Fe	Pt	Fe	Fe	Fe	-519.363	-35.592
Fe	Fe	Pt	Fe	Fe	-519.327	-35.558
Fe	Fe	Fe	Pt	Fe	-519.568	-35.786
Pt	Pt	Fe	Fe	Fe	-515.077	-39.676
Pt	Fe	Pt	Fe	Fe	-515.510	-40.086
Pt	Fe	Fe	Pt	Fe	-516.084	-40.628
Fe	Fe	Fe	Fe	Pt	-513.630	-38.307
Fe	Pt	Pt	Fe	Fe	-514.752	-39.368
Fe	Pt	Fe	Pt	Fe	-514.523	-39.152
Fe	Fe	Pt	Pt	Fe	-513.909	-38.571
Pt	Fe	Fe	Fe	Pt	-508.817	-41.941
Pt	Pt	Pt	Fe	Fe	-509.661	-42.740
Fe	Pt	Fe	Fe	Pt	-508.797	-41.922
Pt	Pt	Fe	Pt	Fe	-509.923	-42.988
Fe	Fe	Pt	Fe	Pt	-508.673	-41.806
Pt	Fe	Pt	Pt	Fe	-509.351	-42.447
Fe	Fe	Fe	Pt	Pt	-509.185	-42.289
Fe	Pt	Pt	Pt	Fe	-508.364	-41.513
Pt	Pt	Fe	Fe	Pt	-503.213	-44.828
Pt	Fe	Pt	Fe	Pt	-503.773	-45.358
Fe	Pt	Pt	Fe	Pt	-504.024	-45.595
Pt	Fe	Fe	Pt	Pt	-504.284	-45.841
Pt	Pt	Pt	Pt	Fe	-503.266	-44.878
Fe	Pt	Fe	Pt	Pt	-504.058	-45.627
Fe	Fe	Pt	Pt	Pt	-502.504	-44.157
Pt	Pt	Pt	Fe	Pt	-497.983	-48.019
Pt	Pt	Fe	Pt	Pt	-498.261	-48.282
Pt	Fe	Pt	Pt	Pt	-497.501	-47.563
Fe	Pt	Pt	Pt	Pt	-497.303	-47.376

9. Figure caption

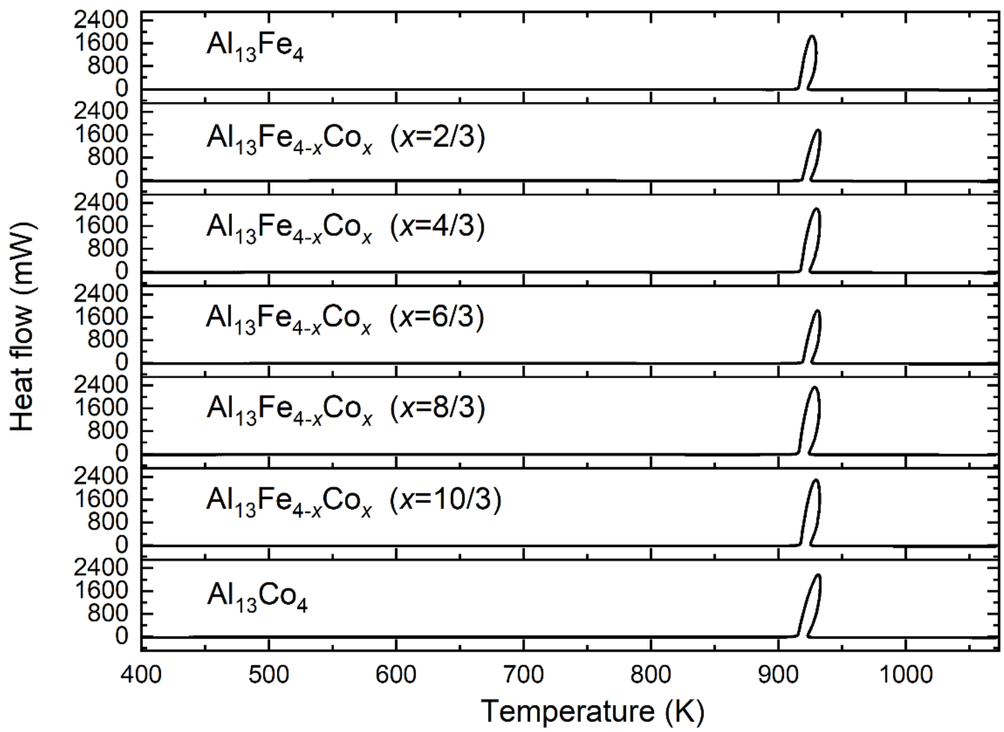

Figure 1: DSC heat-flow signal of in-situ synthesis of the $Al_{13}(Fe,Co)_4$ solid solution at different compositions obtained from a 5 K/min heat ramp of a high purity pure element powders mixture.

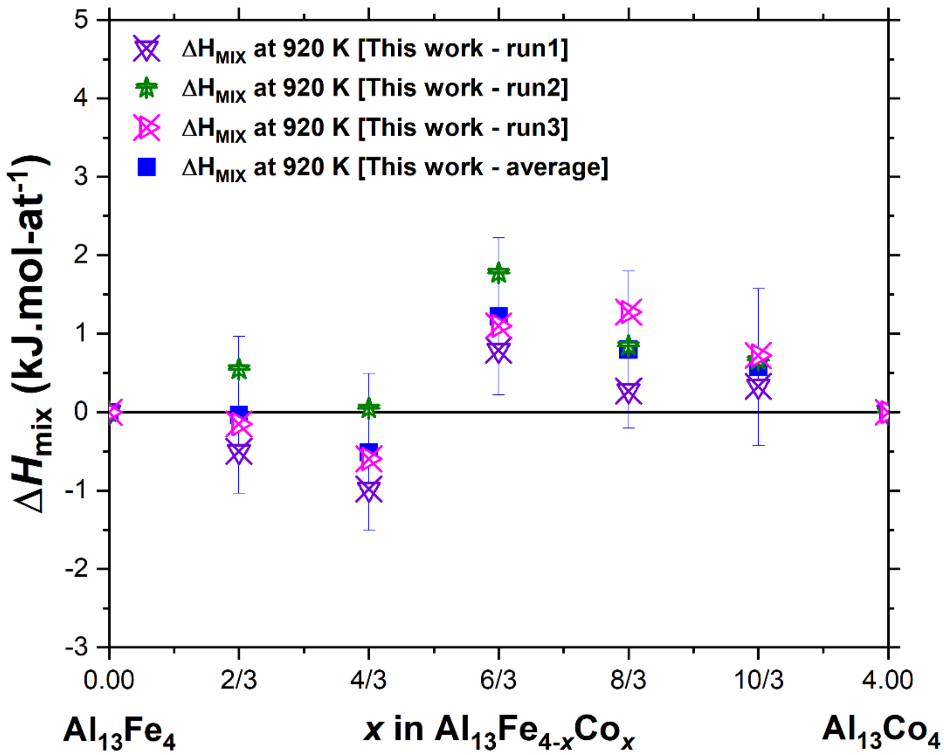

Figure 2: Mixing enthalpy of the $Al_{13}(Fe,Co)_4$ solid solution measured at 920 K by DSC. Reference states are $Al_{13}Fe_4$ and $Al_{13}Co_4$.

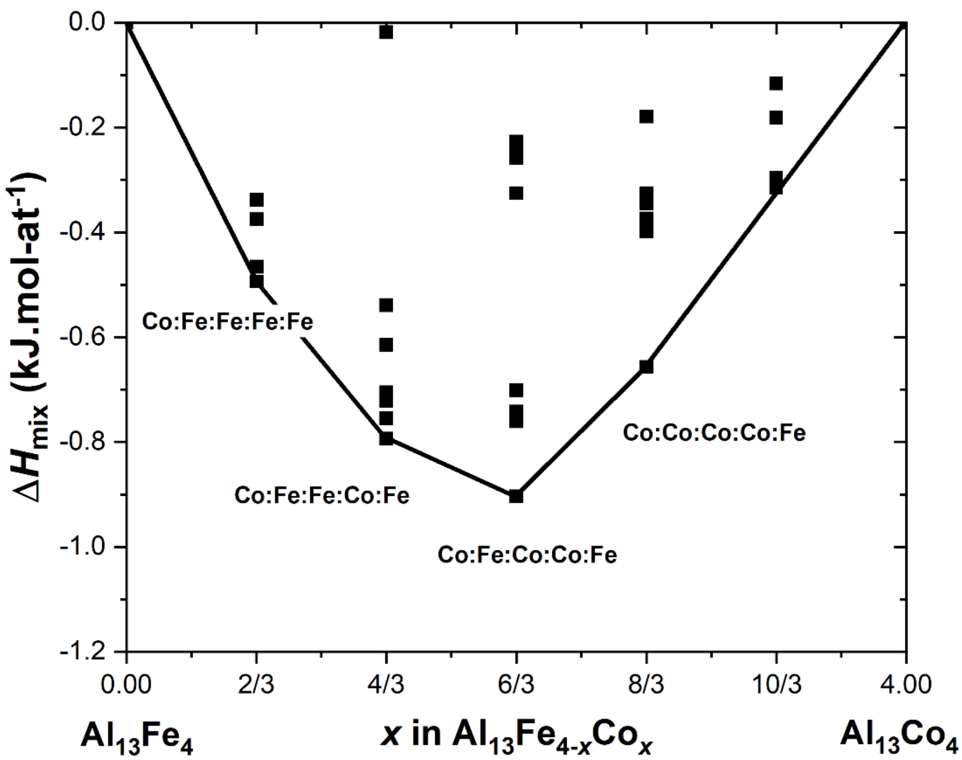

Figure 3: Mixing enthalpy of the $Al_{13}(Fe,Co)_4$ solid solution calculated at 0 K by DFT. The substitution sequence [illegible] A:B:C:D:E means A element on site Fe(1), B element on site Fe(2), etc. Reference states are $Al_{13}Fe_4$ and $Al_{13}Co_4$.

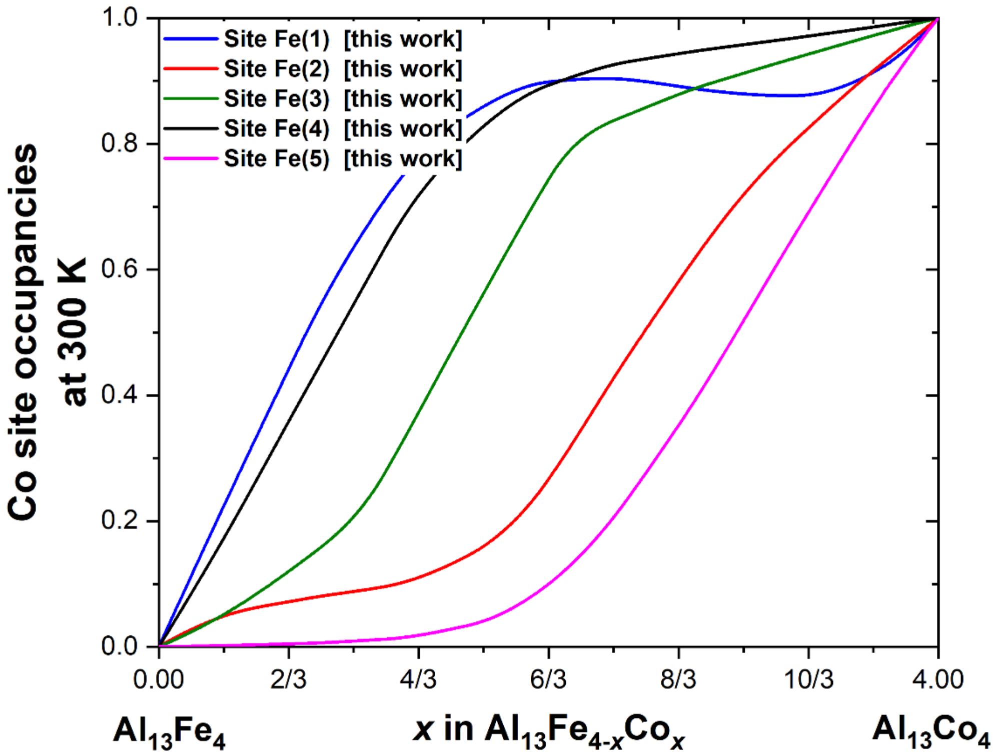

Figure 4: Co site occupancies calculated at 300 K in the $Al_{13}(Fe,Co)_4$ • ' Ž ‹ † • ' Ž — – ‹ ' • ä " ‹ • ï • • ' – ƒ – ‹ ' • ˆ ' " Ž ƒ – – ‹ … is adopted [21].

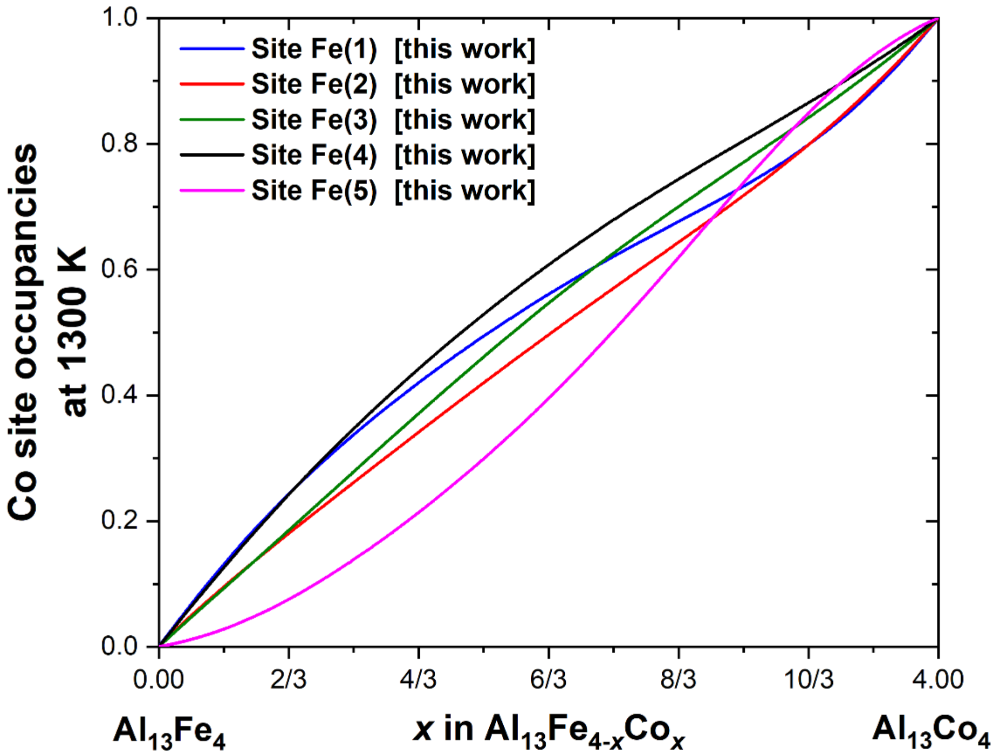

Figure 5: Co site occupancies calculated at 1300 K in the $Al_{13}(Fe,Co)_4$ • ' Ž ‹ † • ' Ž — – ‹ ' • ä " ‹ • ï • • ' – ƒ – ‹ ' • ˆ ' " Ž ƒ – –
sites is adopted [21].

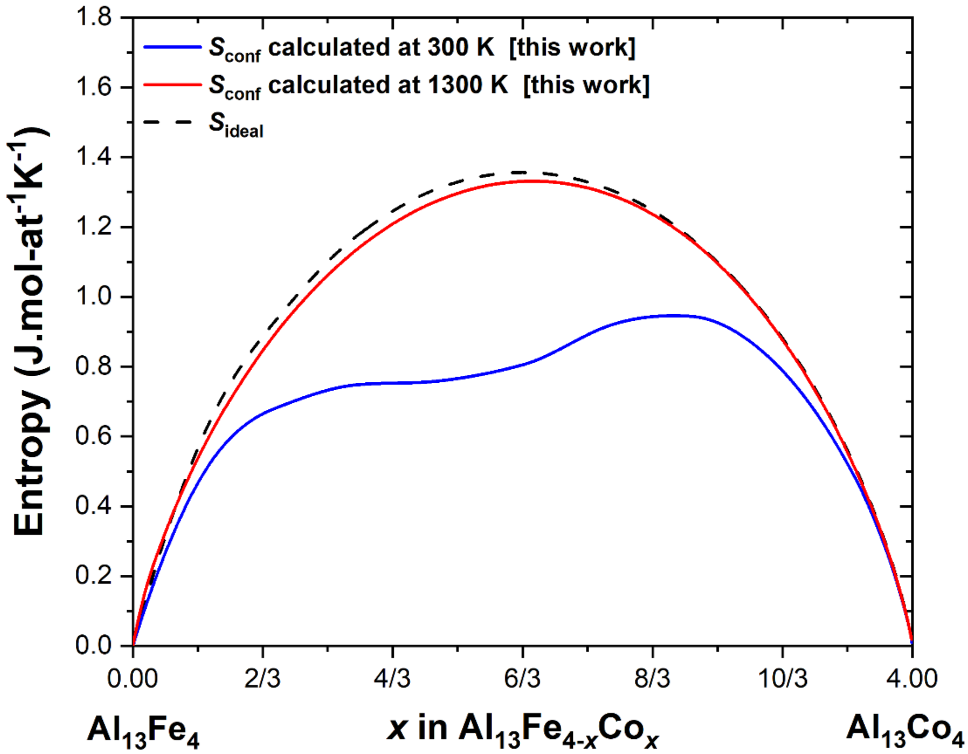

Figure 6: Configurational entropy (S_{conf}) of the $Al_{13}(Fe,Co)_4$ solid solution calculated at 300 K and 1300 K compared to the configurational entropy of an ideal solid solution (S_{ideal}).

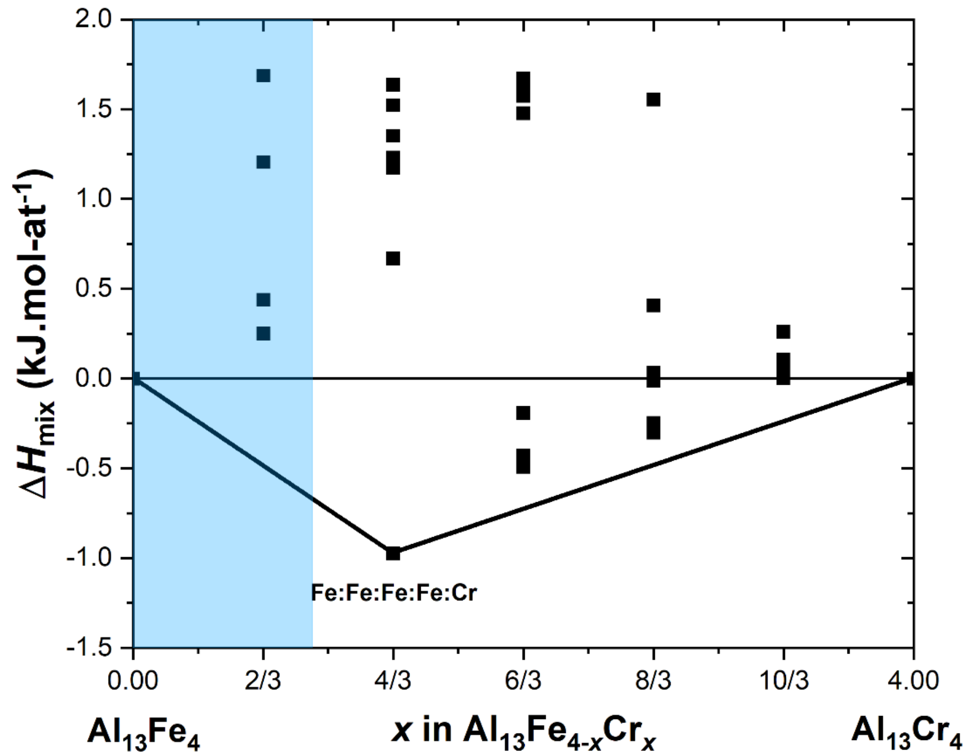

Figure 7: Mixing enthalpy of the $Al_{13}(Fe,Cr)_4$ solid solution calculated at 0K by DFT. The substitution sequence is ”‡’”‡•‡•–‡† ƒ……‘”†‹•‰ –‘ ”‹•ï• •‘–ƒ–‹‘• A:B:C:D:E means A element on site Fe(1), B element on site Fe(2), etc. The maximum homogeneity range of the solid solution is shaded in blue [61]. Reference states are $Al_{13}Fe_4$ and $Al_{13}Cr_4$.

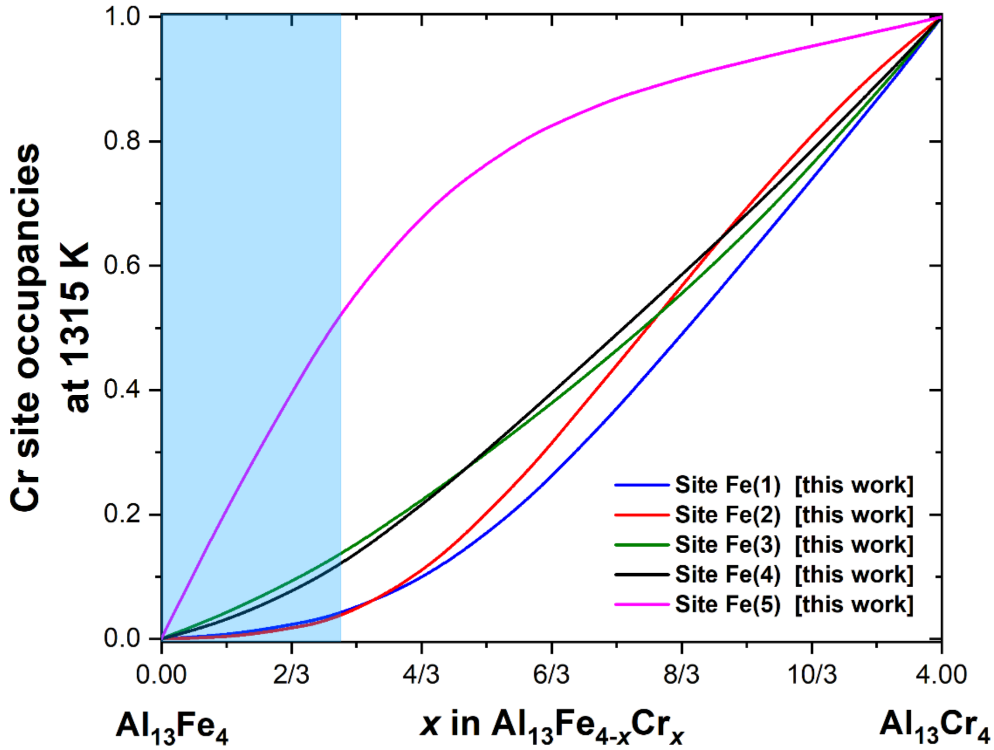

Figure 8: Cr site occupancies calculated at 1315 K in the $Al_{13}(Fe,Cr)_4$ •‘Ž‹† •‘Ž—–‹‘•ä ”‹• ï• •‘–ƒ–‹‘• ˆ‘” Žƒ–– sites is adopted [21]. The maximum homogeneity range of the solid solution is shaded in blue [61].

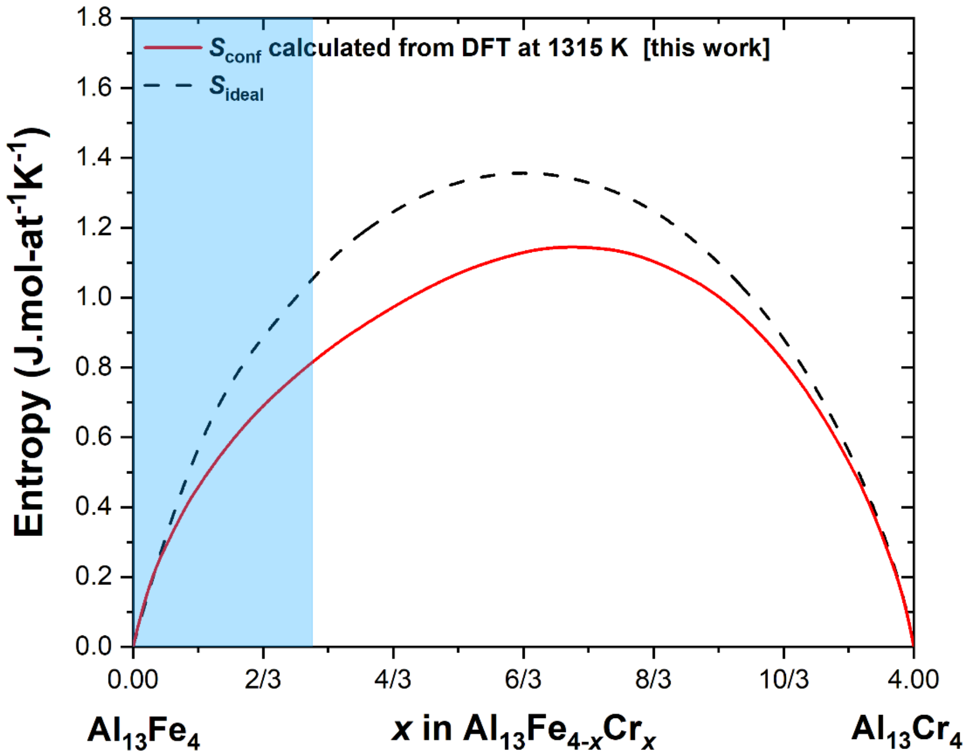

Figure 9: Configurational entropy (S_{conf}) of the $Al_{13}(Fe,Cr)_4$ solid solution calculated at 1315 K compared to the configurational entropy of an ideal solid solution ((S_{ideal})). The maximum homogeneity range of the solid solution is shaded in blue [61].

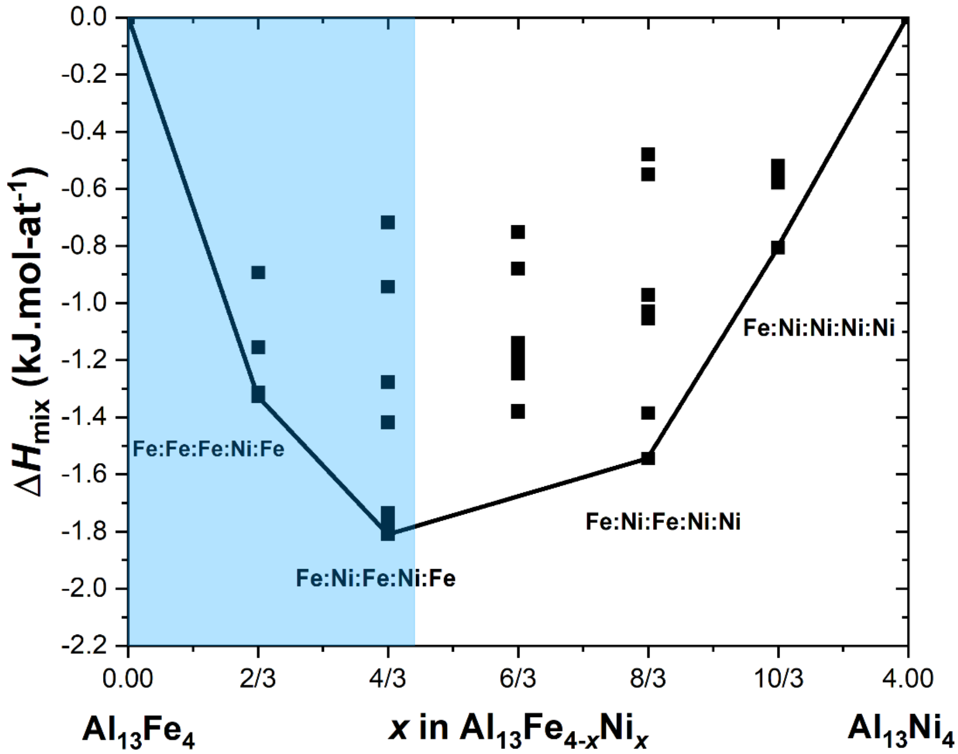

Figure 10: Mixing enthalpy of the $Al_{13}(Fe,Ni)_4$ solid solution calculated at 0 K by DFT. The substitution sequence ‹• ”‡’”‡•‡•–‡† ƒ……‘”†‹•‰ –‘ ”‹ï• •‘–ƒ A:B:C:D:E means A element on site Fe(1), B element on site Fe(2), etc. The maximum homogeneity range of the solid solution is shaded in blue [46]. Reference states are $Al_{13}Fe_4$ and $Al_{13}Ni_4$.

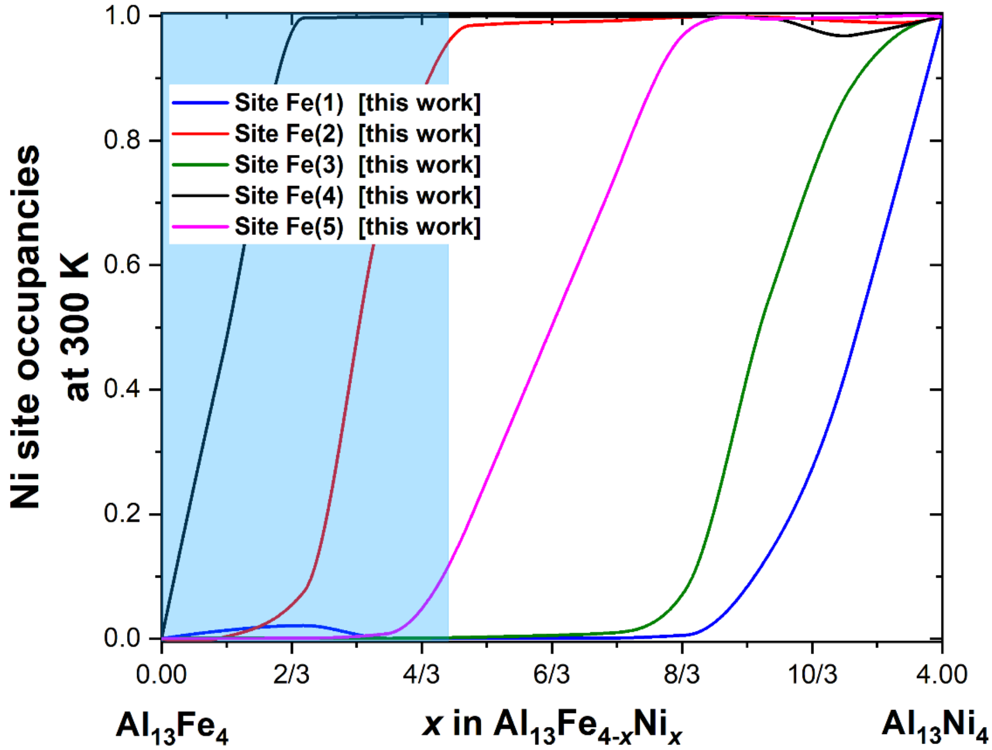

Figure 11: Ni site occupancies calculated at 300 K in the $Al_{13}(Fe,Ni)_4$ •'Ž‹† •'Ž—–‹'•ä ”‹• ï• •'–ƒ–‹'• ˆ'” Žƒ––
sites is adopted [21]. The maximum homogeneity range of the solid solution is shaded in blue [46].

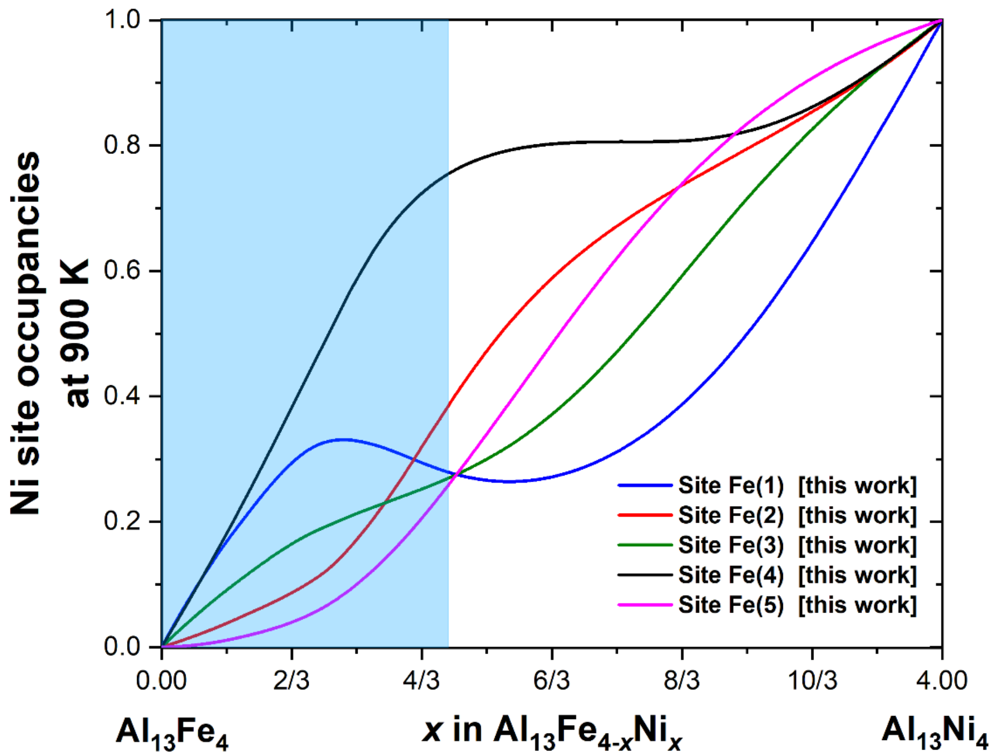

Figure 12: Ni site occupancies calculated at 900 K in the $Al_{13}(Fe,Ni)_4$ •‘Ž‹† •‘Ž——‹‘•ä ”‹• ï• •‘–ƒ–‹‘• ˆ‘” Žƒ––
sites is adopted [21]. The maximum homogeneity range of the solid solution is shaded in blue [46].

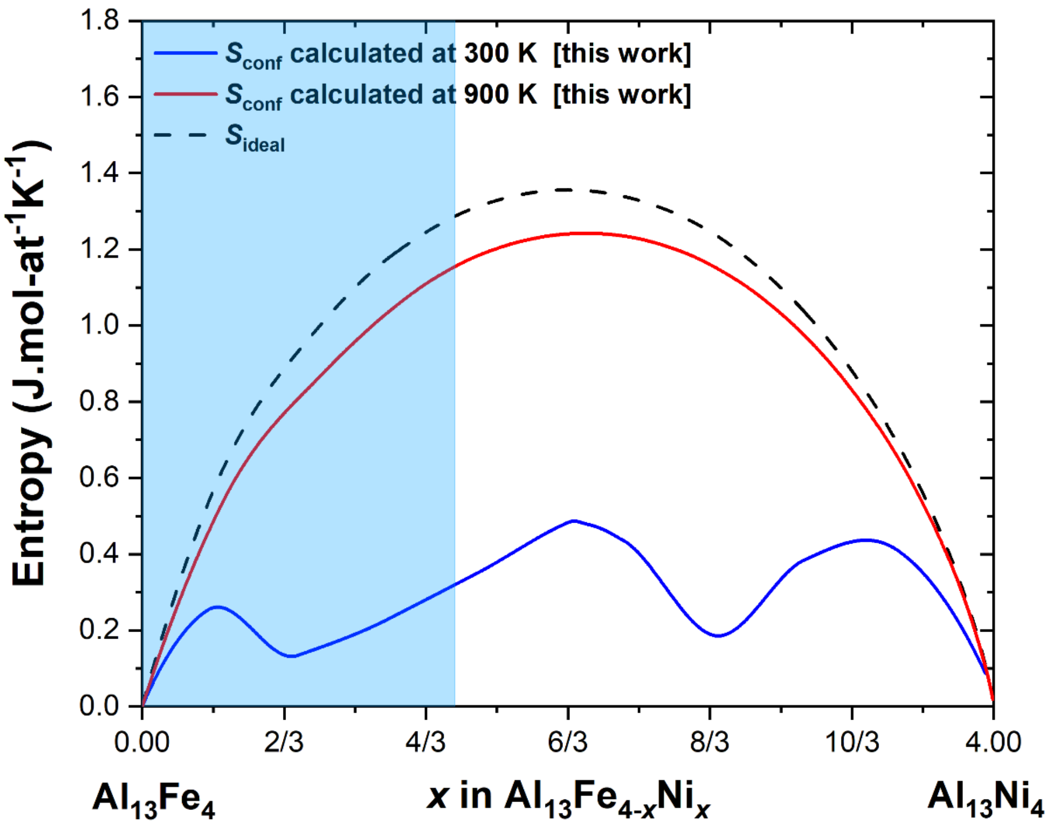

Figure 13: Configurational entropy (S_{conf}) of the $Al_{13}(Fe,Ni)_4$ solid solution calculated at 300 K and 900 K compared to the configurational entropy of an ideal solid solution ((S_{ideal})). The maximum homogeneity range of the solid solution is shaded in blue [46].

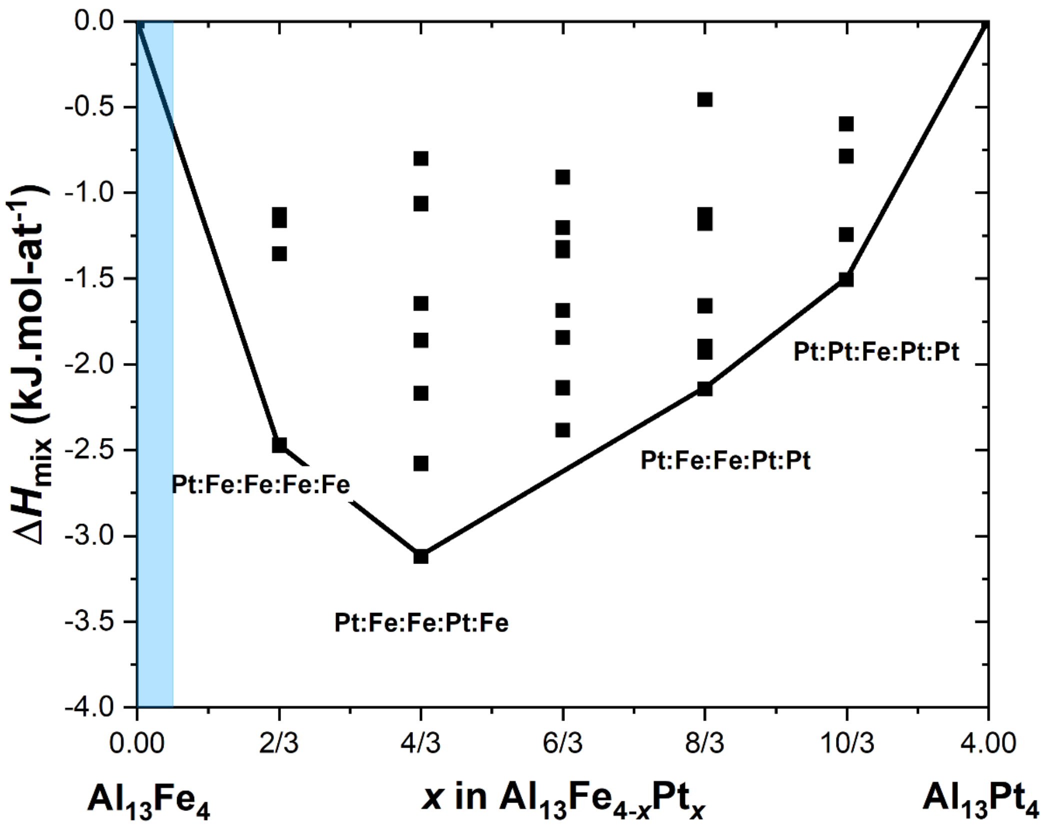

Figure 14: Mixing enthalpy of the $Al_{13}(Fe,Pt)_4$ solid solution calculated at 0 K by DFT. The substitution sequence ‹• ”‡’”‡•‡•–‡† ƒ…… ‘”†‹•‰ –‘ ”‹•ï• •‘–ƒ–‹‘: A:B:C:D:E means A element on site Fe(1), B element on site Fe(2), etc. The maximum homogeneity range of the solid solution is shaded in blue [48]. Reference states are $Al_{13}Fe_4$ and $Al_{13}Pt_4$.

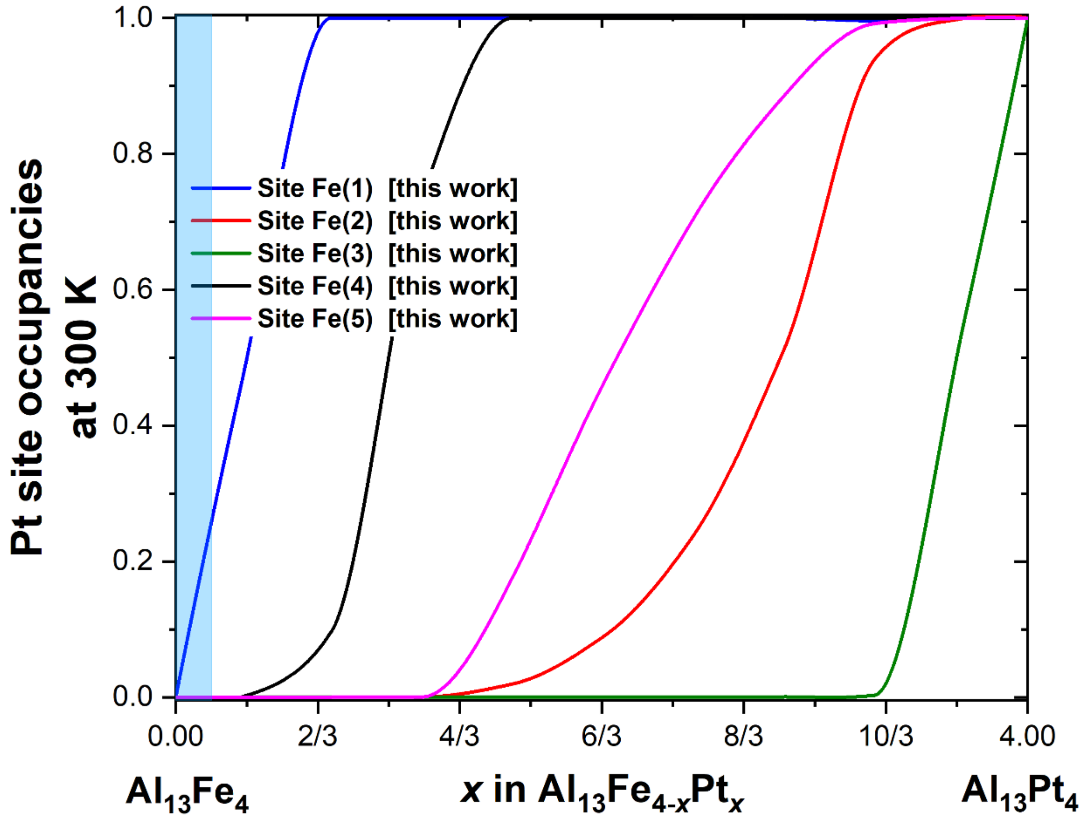

Figure 15: Pt site occupancies calculated at 300 K in the $Al_{13}(Fe,Pt)_4$ •'Ž‹† •'Ž—–‹'•ä ”‹• ï• •'–ƒ–‹'• ˆ'” Žƒ––‹ is adopted [21]. The maximum homogeneity range of the solid solution is shaded in blue [48].

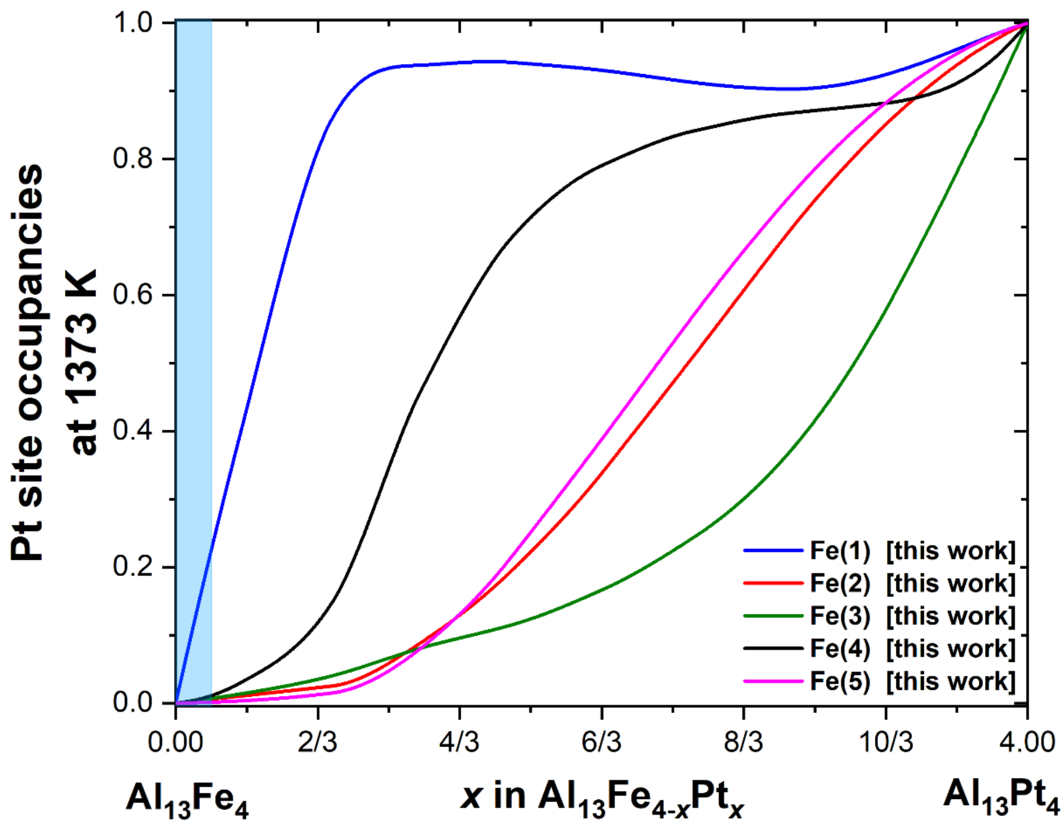

Figure 16: Pt site occupancies calculated at 1373 K in the $Al_{13}(Fe,Pt)_4$ • ' Ž ‹ † • ' Ž — – ‹ ' • ä " ‹ • ï • • ' – ƒ – ‹ ' • ˆ ' " Ž ƒ – – ‹ is adopted [21]. The maximum homogeneity range of the solid solution is shaded in blue [48].

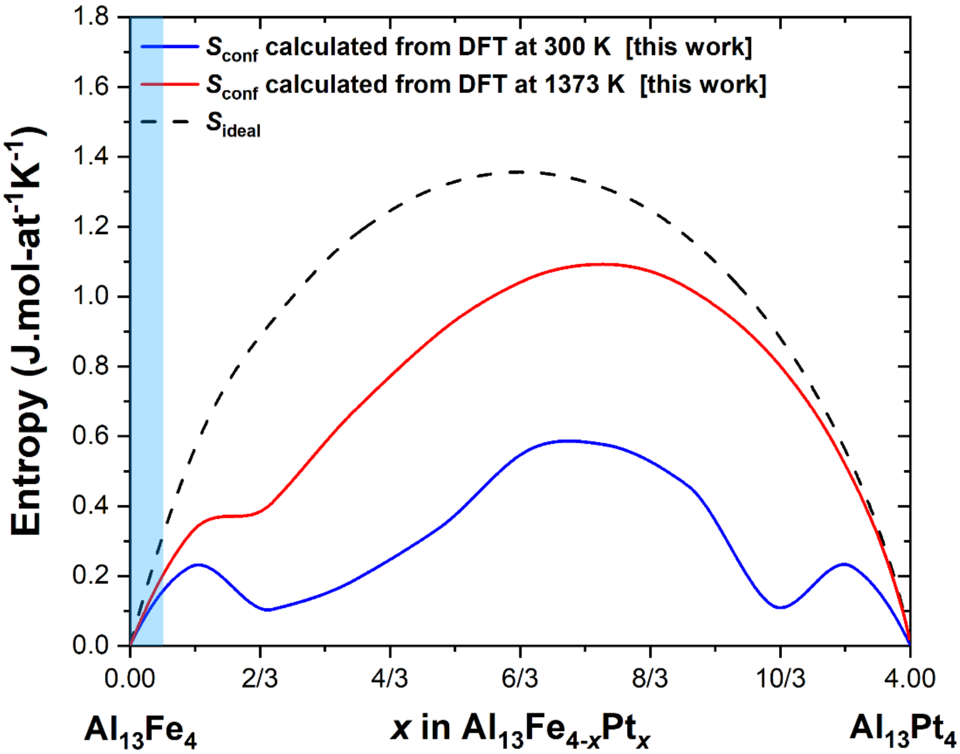

Figure 17: Configurational entropy (S_{conf}) of the $Al_{13}(Fe,Pt)_4$ solid solution calculated at 300 K and 1373 K compared to the configurational entropy of an ideal solid solution ((S_{ideal})). The maximum homogeneity range of the solid solution is shaded in blue [48].

10. Appendix

Table 8: Optimised parameter of the $Al_{13}(Fe,Co)_4$ solid solution

		Site multiplicity				Parameter (J/mol)
Al(1-15)	Fe(1)	Fe(2)	Fe(3)	Fe(4)	Fe(5)	
78	4	4	4	4	8	
Al	Fe	Fe	Fe	Fe	Fe	-3.6735E6+7098*T-1251*TLn(T)-3.54*T2+1.224E-3*T3-2.6045E-7*
Al	Co	Co	Co	Co	Co	-4.2602E6+7057*T-1251*TLn(T)-3.48*T2+1.224E-3*T3-2.6045E-7*
Al	Co	Fe	Fe	Fe	Fe	-3.8354E6+7377*T-1291*TLn(T)-3.56*T2+1.224E-3*T3-2.6045E-7*
Al	Fe	Co	Fe	Fe	Fe	-3.8229E6+7377*T-1291*TLn(T)-3.56*T2+1.224E-3*T3-2.6045E-7*
Al	Fe	Fe	Co	Fe	Fe	-3.8192E6+7377*T-1291*TLn(T)-3.56*T2+1.224E-3*T3-2.6045E-7*
Al	Fe	Fe	Fe	Co	Fe	-3.8322E6+7377*T-1291*TLn(T)-3.56*T2+1.224E-3*T3-2.6045E-7*
Al	Co	Co	Fe	Fe	Fe	-3.9440E6+7364*T-1291*TLn(T)-3.54*T2+1.224E-3*T3-2.6045E-7*
Al	Co	Fe	Co	Fe	Fe	-3.9582E6+7364*T-1291*TLn(T)-3.54*T2+1.224E-3*T3-2.6045E-7*
Al	Co	Fe	Fe	Co	Fe	-3.9662E6+7364*T-1291*TLn(T)-3.54*T2+1.224E-3*T3-2.6045E-7*
Al	Fe	Fe	Fe	Fe	Co	-3.8832E6+7364*T-1291*TLn(T)-3.54*T2+1.224E-3*T3-2.6045E-7*
Al	Fe	Co	Co	Fe	Fe	-3.9363E6+7364*T-1291*TLn(T)-3.54*T2+1.224E-3*T3-2.6045E-7*
Al	Fe	Co	Fe	Co	Fe	-3.9550E6+7364*T-1291*TLn(T)-3.54*T2+1.224E-3*T3-2.6045E-7*
Al	Fe	Fe	Co	Co	Fe	-3.9532E6+7364*T-1291*TLn(T)-3.54*T2+1.224E-3*T3-2.6045E-7*
Al	Co	Fe	Fe	Fe	Co	-4.0053E6+7376*T-1291*TLn(T)-3.56*T2+1.224E-3*T3-2.6045E-7*
Al	Co	Co	Co	Fe	Fe	-4.0054E6+7376*T-1291*TLn(T)-3.56*T2+1.224E-3*T3-2.6045E-7*
Al	Fe	Co	Fe	Fe	Co	-4.0073E6+7376*T-1291*TLn(T)-3.56*T2+1.224E-3*T3-2.6045E-7*
Al	Co	Co	Fe	Co	Fe	-4.0598E6+7376*T-1291*TLn(T)-3.56*T2+1.224E-3*T3-2.6045E-7*
Al	Fe	Fe	Co	Fe	Co	-4.0085E6+7376*T-1291*TLn(T)-3.56*T2+1.224E-3*T3-2.6045E-7*
Al	Co	Fe	Co	Co	Fe	-4.0744E6+7376*T-1291*TLn(T)-3.56*T2+1.224E-3*T3-2.6045E-7*
Al	Fe	Fe	Fe	Co	Co	-4.0153E6+7376*T-1291*TLn(T)-3.56*T2+1.224E-3*T3-2.6045E-7*
Al	Fe	Co	Co	Co	Fe	-4.0578E6+7376*T-1291*TLn(T)-3.56*T2+1.224E-3*T3-2.6045E-7*
Al	Co	Co	Fe	Fe	Co	-4.0980E6+7365*T-1290*TLn(T)-3.54*T2+1.224E-3*T3-2.6045E-7*
Al	Co	Fe	Co	Fe	Co	-4.1129E6+7365*T-1290*TLn(T)-3.54*T2+1.224E-3*T3-2.6045E-7*
Al	Fe	Co	Co	Fe	Co	-4.1149E6+7365*T-1290*TLn(T)-3.54*T2+1.224E-3*T3-2.6045E-7*
Al	Co	Fe	Fe	Co	Co	-4.1178E6+7365*T-1290*TLn(T)-3.54*T2+1.224E-3*T3-2.6045E-7*
Al	Co	Co	Co	Co	Fe	-4.1474E6+7365*T-1290*TLn(T)-3.54*T2+1.224E-3*T3-2.6045E-7*
Al	Fe	Co	Fe	Co	Co	-4.1204E6+7365*T-1290*TLn(T)-3.54*T2+1.224E-3*T3-2.6045E-7*
Al	Fe	Fe	Co	Co	Co	-4.1192E6+7365*T-1290*TLn(T)-3.54*T2+1.224E-3*T3-2.6045E-7*
Al	Co	Co	Co	Fe	Co	-4.1896E6+7362*T-1291*TLn(T)-3.54*T2+1.224E-3*T3-2.6045E-7*
Al	Co	Co	Fe	Co	Co	-4.1963E6+7362*T-1291*TLn(T)-3.54*T2+1.224E-3*T3-2.6045E-7*
Al	Co	Fe	Co	Co	Co	-4.2079E6+7362*T-1291*TLn(T)-3.54*T2+1.224E-3*T3-2.6045E-7*
Al	Fe	Co	Co	Co	Co	-4.2111E6+7362*T-1291*TLn(T)-3.54*T2+1.224E-3*T3-2.6045E-7*

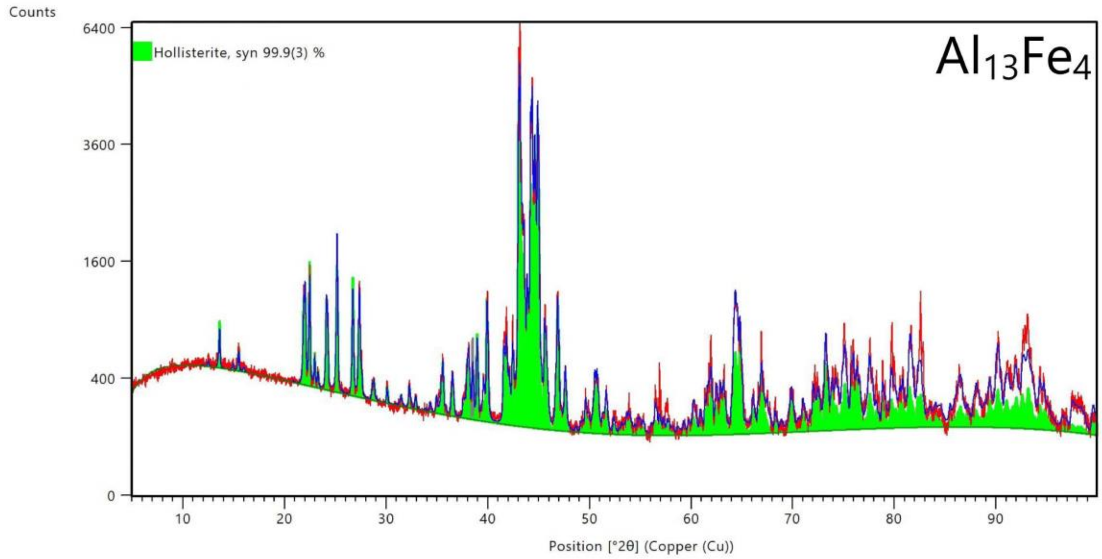

Figure 18: Rietveld refinement of $Al_{13}Fe_4$ (sample #1). Experimental (red) and calculated (blue) patterns are shown. The proportion quantification of each phase is shown in green.

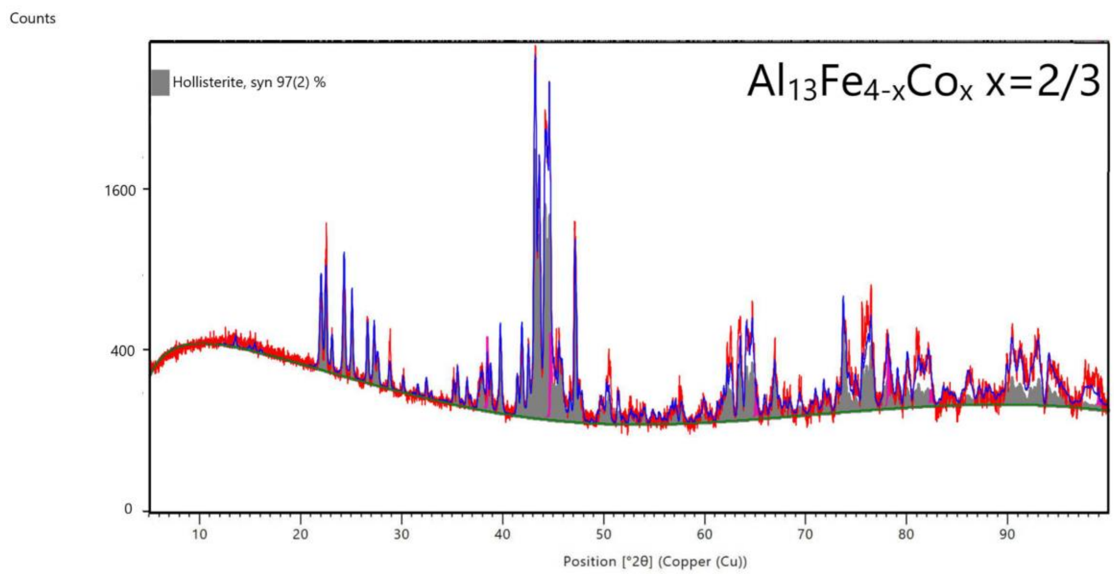

Figure 19: Rietveld refinement of $Al_{13}Fe_{4-x}Co_x$ ($x = 2/3$) (sample #2). Experimental (red) and calculated (blue) patterns are shown. The proportion quantification of each phase is shown in grey.

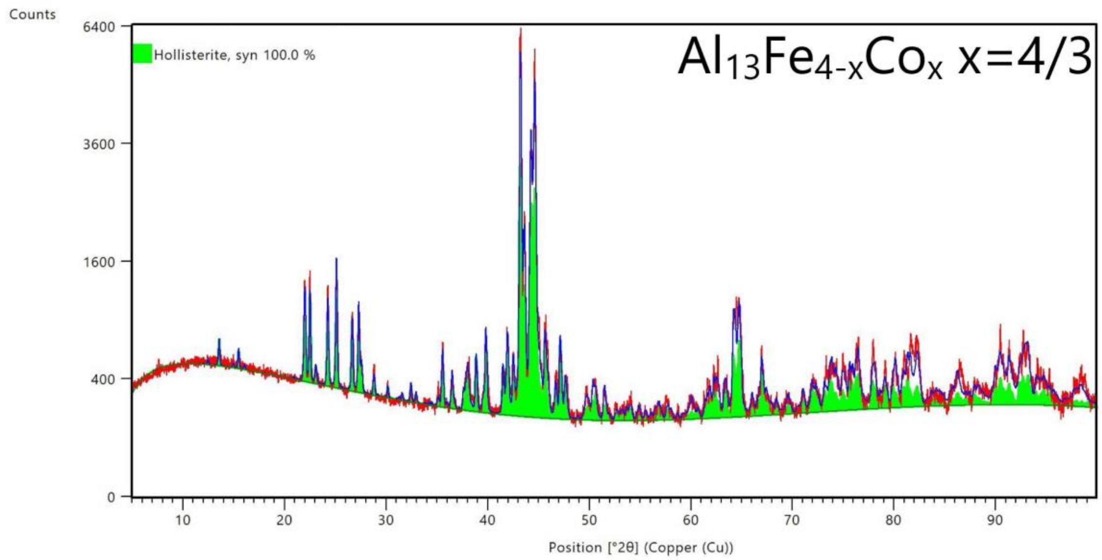

Figure 20: Rietveld refinement of $Al_{13}Fe_{4-x}Co_x$ ($x = 4/3$) (sample #3). Experimental (red) and calculated (blue) patterns are shown. The proportion quantification of each phase is shown in green.

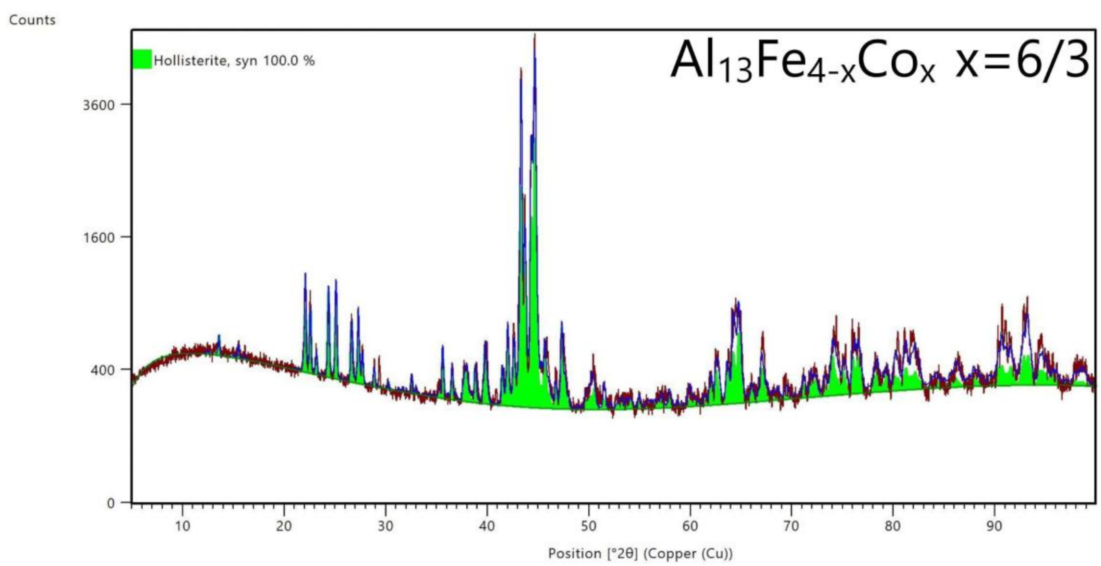

Figure 21: Rietveld refinement of $Al_{13}Fe_{4-x}Co_x$ ($x = 6/3$) (sample #4). Experimental (red) and calculated (blue) patterns are shown. The proportion quantification of each phase is shown in green.

Figure 22: Rietveld refinement of $Al_{13}Fe_{v\,x}Co_x$ ($x = 8/3$) (sample #5). Experimental (red) and calculated (blue) patterns are shown. The proportion quantification of each phase is shown in green.

Figure 23: Rietveld refinement of $Al_{13}Fe_{v\,x}Co_x$ ($x = 10/3$) (sample #6). Experimental (red) and calculated (blue) patterns are shown. The proportion quantification of each phase is shown in green.

Figure 24: Rietveld refinement of $Al_{13}Co_4$ (sample #7). Experimental (red) and calculated (blue) patterns are shown. The proportion quantification of each phase is shown in grey.